Projection of the Airborne CO2 Concentration by Land/Ocean Absorption Dynamics and Fossil-Fuel Reserve Depletion

Environmental Modeling & Assessment (2024) 29:1167–1187
https://doi.org/10.1007/s10666-024-09985-7

RESEARCH

Projection of the Airborne CO_2 Concentration by Land/Ocean Absorption Dynamics and Fossil-Fuel Reserve Depletion

Enrico Canuto[2] · Daniele Mazza[2] · Carlo Novara[1]

Received: 23 November 2022 / Accepted: 6 June 2024 / Published online: 13 July 2024

Abstract
The paper has been suggested by the following observations: (1) the atmospheric growth rate of carbon dioxide concentration is smaller than that ascribed to the emission of fossil-fuel combustion and (2) the fossil-fuel reserves are finite. The first observation leads to a simple dynamic model, based on the balance of CO_2 land/ocean absorption and anthropogenic emissions, only limited by the depletion of fossil-fuel reserves, in a business-as-usual scenario. The second observation suggests of projecting the past CO_2 emissions to the future, by constraining emissions to the limit of reserve availability. Similar projections are available in the literature, but either driven by heuristics or by complex simulation packages. The paper provides a simple and formal method only driven by historical data, their uncertainty and simple models. The method aims to provide CO_2 concentration projections, which being constrained by fossil-fuel finite reserve may be in principle employed as bounds to forecasting exercises. The time–invariant dynamics of the land/ocean absorption is the simplification of a more complex set of equations describing carbon dioxide exchange between different reservoirs. Contribution of other greenhouse gases like methane and nitrous oxide has been neglected, since their emissions cannot be projected with the paper methodology. Comparison with recent profiles of the Intergovernmental Panel on Climate Change (IPCC) confirms that the finite-reserve projections of the fossil fuel emissions is close to those of a moderate Shared Socioeconomic Scenario (SSP) like SSP2-4.5—a result in agreement with other authors—but also reveals the limits of the simplified model, when extending the tuned dynamics of the recent mean CO_2 exchanges to long-term future. The limits derive from linearity, time invariance, and aggregation assumptions, which allow a more complex model of CO_2 exchanges to be simplified and tuned on experimental data.

Keywords Airborne CO_2 · CO_2 concentration · Fossil-fuel emission · Fossil-fuel reserve · CO_2 land/ocean absorption dynamics · CO_2 projection

1 Introduction

Future greenhouse gas (GHG) and especially carbon dioxide (CO_2) emissions by fossil-fuel combustion are the subject of extensive research, in relationships with international pledges about net zero 2050 emissions [1]. The Intergovernmental Panel on Climate Change (IPCC) already in 1990 assessed long-term emission scenarios up to 2100 [2]. These scenarios have been used in the analysis of the possible change of climate variables (especially the climate energy measured by the global near-surface temperature) due to increasing atmospheric GHG concentration and of the options for mitigating the change. Recently the Climate Action Tracker (CAT, [3]) has summarized in a chart the projections of different policies aiming at reducing the atmospheric concentration growth of carbon dioxide and other GHGs, in an effort of mitigating the relevant effects on future global warming. Revised scenarios and projections, included in Figure TS.4, page 53, of the Technical Summary in [4], are compared with the paper findings in Section 4.2.

The above cited scenarios and simulations (see [5–8], and [9]) do not explicitly mention, as a limiting factor

✉ Carlo Novara
carlo.novara@polito.it

Enrico Canuto
enrico.canuto@formerfaculty.polito.it

Daniele Mazza
mazzad50@gmail.com

[1] Dipartimento di Elettronica e Telecomunicazioni, Politecnico di Torino, Corso Duca Degli Abruzzi 24, 10129 Turin, Italy

[2] Former faculty, Politecnico di Torino, Turin, Italy

of the fossil-fuel emissions, their physical reserves. The topic of "fossil-fuel resources ('reserves' in this paper) as a constraint in emissions scenarios" is explicitly treated in [10–13], and [14]. In [10], literature projections are compared with the IPCC Representative Concentration Pathways (RCP) in [15]. In [14], fossil-fuel emission and reserve data are elaborated by a logistic equation to project future emissions. Other publications like [16] and [17] treat this topic with the aim of predicting the amount of reserves that will remain unextracted under IPCC mitigation strategies.

The goal of the paper is to offer a complete, formal, and statistically proven procedure for converting historical CO_2 concentration and emission data into a simple dynamic model that allows measurements to be projected into the future, while respecting the constraint of finite fossil-fuel reserves. The procedure may be repeated by scholars, fed by new data and gradually enriched by other data, in agreement with the more complex model of the Appendix.

The paper starts from the airborne CO_2 concentration, which has been measured by the Mauna Loa Observatory since 1958 (the so-called Keeling curve [18]), thus neglecting other GHGs like methane and nitrous oxide as they depend on different emission sources and removal mechanisms. The CO_2 concentration is defined as the mole fraction in a given volume of the dry air [19]. It is referred to by IPCC as mixing ratio in the Glossary [20]. The concentration unit, which is employed here, is the part per million of the mole fraction, shortened to [ppm]. The conversion between mass and mole fraction is explained in Section 2.2. CO_2 is dynamically exchanged among atmosphere, biomass, land and ocean, in the so-called annual carbon cycle (see [21, 22], and [23]). A big deal of carbon dioxide is taken out from atmosphere by vegetation photosynthesis, but at the same time, half of this goes back to air by vegetation emission during night and by daily animal breathing. Part of the remainder goes to soil after vegetation death and, due to bacterial fermentation, again into the air. Part is washed away by surface fresh water into the sea. An estimate of the net exchange can be performed by computerized models. Their results have been collected by the Global Carbon Project (GCP, [24, 25]).

Before industrial era, ice-core proxy data of the last 2000 years, show the concentration of the airborne CO_2 fluctuating around 280 ± 10 ppm [21]. The concentration, since the early nineteenth century, is slowly growing until World War II, and then steadily increasing since the fifties of the past century, when systematic measurements began to be provided by the Mauna Loa Observatory (data have been retrieved from the Scripps Research site [26]). As a result, the seasonal exchange between land, ocean, and atmosphere is accompanied by a mean atmospheric increase, small if compared with the seasonal exchange, but progressively accumulating. The main contribution to such an inflow has been allotted, less than one century ago [27], to the CO_2 emission of the fossil-fuel combustion [21, 28]. Actually, the mean annual emission flow [ppm/y] happens to be larger than the corresponding airborne concentration growth, as shown in Fig. 1a, implying that part of the accumulated carbon dioxide is absorbed by land and ocean, which behave as carbon sinks. In Fig. 1a, the cumulative fossil–fuel emission [ppm] is the progressive sums of the annual emissions [ppm/y] during the industrial era (since 1750). It is compared with the airborne CO_2 concentration increment during the same period. Figure 1b shows the annual rate [ppm/y] of the concentration profiles in Fig. 1a.

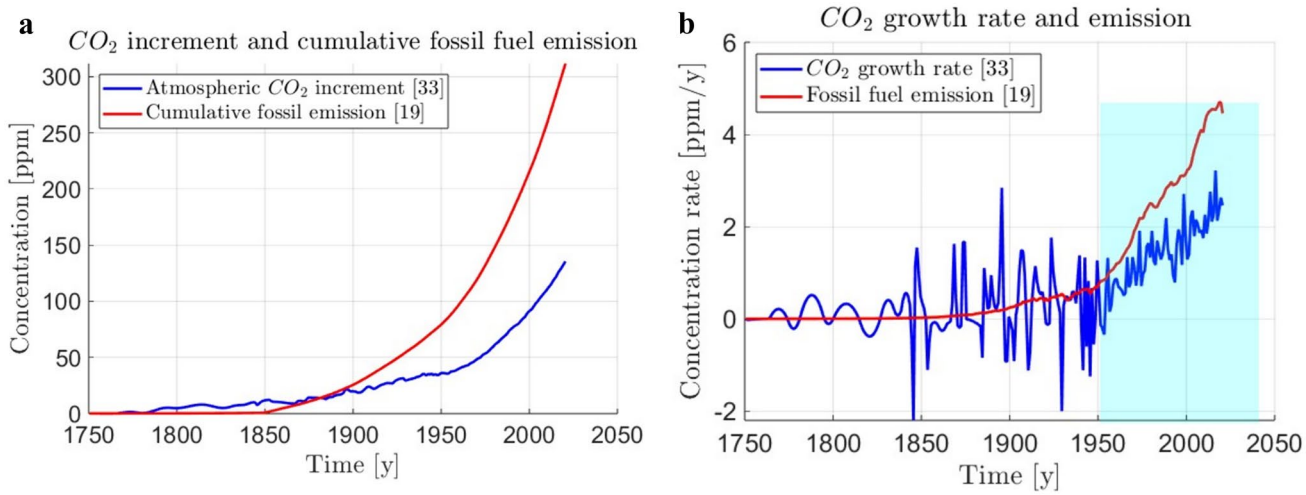

Fig. 1 **a** Annual airborne CO_2 concentration since 1750 (from Scripps Research [26]) and cumulative fossil-fuel emission (from Global Carbon Project [24]). **b** Annual rate of the profiles in (**a**): the CO_2 growth rate and the fossil-fuel emission

A fundamental question arises: How long does it take a perturbation of the airborne CO_2 to be absorbed by land and ocean sinks? Answer to this question will be given in Sect. 2, with the aim of forecasting the future CO_2 concentration based on the proposed dynamic model. The absorption time constant (the term is typical of the dynamic system field [29], relaxation time of chemistry [30]) should not be confused, as pointed out in [21, 31], and [32], with the residence time driven by the annual land/ocean–atmosphere zero-mean flow. In terms of dynamic systems, the latter is the CO_2 transport delay in the atmosphere, like that of a fluid along a pipe. Both time intervals are referred to as lifetimes by [21]. Their origin is different: chemistry kinetics at the boundary between land/ocean and atmosphere in the former case, atmospheric transport mechanisms in the latter case.

A better distinction between absorption time constant and residence time may be provided by fixed-volume (Eulerian) fluid dynamics (see the Appendix) and parcel (Lagrangian) fluid dynamics. The fluid level $x(t)$ in a fixed volume (e.g. CO_2 concentration in a given dry-air volume) is the result of the flows from/to the environment. By restricting to a small perturbation $\delta x(t) = x(t) - \underline{x}$ around a constant equilibrium level $\underline{x}$, the equilibrium is said to be asymptotically stable if and only if the input/output flow balance contains (i) a *negative feedback term* $-k\delta x(t), k > 0$, whose positive opposite $k\delta x(t)$, under $\delta x(t) > 0$, represents the land/ocean absorption of the airborne CO_2, and (ii) a flow balance $u(t)$ independent of $\delta x(t)$, according to the state equation: $\delta\dot{x}(t) = -k\delta x(t) + u(t), \delta x\left(t_0\right) = \delta x_0$. The parameter $\tau = \frac{1}{k}$[s] is referred here as *absorption time constant*, thinking to the absorption of the airborne CO_2 by land and ocean, because of $\delta x(t) > 0$, with respect to a pre-industrial equilibrium $\underline{x}$. The time constant has been estimated in [21] equal to 100 years and in this paper (Section 2.5) to about 50 years. The flow term $u(t)$ may be split into four terms: (i) a zero-mean bounded periodic term, which is dominated by the annual carbon flow (neglected in the paper by taking the annual mean of the previous state equation); (ii) an unbounded term, which is dominated by anthropogenic CO_2 emissions (treated in the paper); (iii) a bounded terms dominated by the anthropogenic land-use change emission (treated in the paper); and (iv) bounded irregular terms (treated in the paper). Coming to Lagrangian dynamics, let us consider a CO_2 parcel emitted by land and ocean. While in the atmosphere, it will be transported, transformed and dispersed, and then reconstituted. The time taken by a mean CO_2 parcel to come back to land and ocean is referred to as *airborne residence time*: It has been estimated in [21] equal to 3.5 years. The annual periodic component of $u(t)$ is the main responsible.

Several packages of global circulation models (GCM) have been devoted to simulate and understand the Earth's carbon cycle within the studies of the global climate prediction. The paper derives a simple dynamic model of the annual mean carbon cycle mimicking the chemical kinetics of the carbon dioxide exchanged between atmosphere and land and atmosphere and ocean. The model is described in the Appendix as a set of state equations, where each state variable accounts for the CO_2 amount of Earth's reservoirs (as such or in chemically modified forms), included the fossil-fuel deposits (coal, oil and natural gas). Model simplification under reasonable assumptions leads to a first-order differential equation with a pair of unknown parameters:

1. The equilibrium $\underline{x}$ of the airborne CO_2 concentration is found close to the ice-core mean value of the last two Holocene millennia.
2. The time constant τ of the stabilizing land/ocean absorption feedback is found close to half a century. The estimated time constant includes the effect of the carbon feedback [21], which, by opposing land/ocean absorption, is such to increase τ.

Advantages of simple physical models can be summarized as follows: (i) parameters can be easily related to historical data; (ii) model structure can be statistically checked and optimized; (iii) they provide intuitive interpretation of the involved phenomena; and (iv) they may provide, if properly constructed, identified and validated, reasonable predictions of the phenomenon of interest.

In [14], fossil-fuel emissions, similar to those in Section 3, are projected by means of a modified logistic equation. The author relies on a public domain model like MAGICC (Model for the Assessment of Greenhouse Gas Induced Climate Change, described in [33]) for integrating emission data into the airborne CO_2 concentration. The interesting fact is that peak values and times of CO_2 emission and concentration in [14] look rather close to the findings of this paper as reported in Table 5, thus providing a check.

Estimation of the dynamic model parameters in Sections 2 and 3 from experimental data and the subsequent projections in Section 4 look close to the practice in the carbon cycle and climate change literature. For instance, in [34–36], and [37], starting from projections of GCM packages, the main goal was to identify the carbon feedback gain and constituent parameters. Their procedure exploits static relations between airborne and land/ocean CO_2 concentration, cumulative emissions, and global temperature, which can be rewritten in terms of the Appendix model, as briefly shown in Section 2.7.

In Section 3, historical data of the fossil-fuel depletion are predicted with the help of the Meixner distribution (see [38] and [39]), a typical bell-shaped curve. As explained in Section 3.3, the choice among similar curves comes from the direct interpretation of the Meixner distribution parameters in terms of the prediction amplitude, shape, skewness, and

Table 1 CO_2 reservoirs and their notations

No.	Reservoir	Symbols	Unit (alternative)	State equation	Comments
1	Atmosphere	x_1, x	ppm ($GtCO_2$)	(10), (A.18)	Absorption dynamics
2	Ocean	x_2	ppm ($GtCO_2$)	(A.8)	Appendix
3	Land (vegetation and soil)	x_3	ppm ($GtCO_2$)	(A.8)	Appendix
4	Cement constructions	x_4	ppm ($GtCO_2$)	(A.8)	Appendix
5	Fossil fuels	x_5, r	ppm ($GtCO_2$)	(24), (A.18)	Emission projection
6	Total	x_0	ppm ($GtCO_2$)	(A.1)	Appendix
7	Earth's interior	NA	Not available (NA)	NA	Neglected
8	Fossil-fuel emission	$c = u_5$	$GtCO_2$/y (ppm/y)	(24), (A.18)	Emission projection
9	Fossil-fuel emission	$u = u_5$	$GtCO_2$/y (ppm/y)	(10), (A.18)	Absorption dynamics

location. The aim is to predict a future depletion that is constrained by current reserves. The predicted depletion, converted into equivalent CO_2 emission, becomes the input of the absorption dynamic model. Starting from the current epoch, the model integrates the predicted emissions, decremented by land and ocean absorption, thus providing a finite-reserve projection of the airborne CO_2 concentration until $t_{End} = 2150$ y. The date has been chosen both for accommodating coal reserves and for agreeing with the model validity interval, from $t_0 = 1955$ y to $t_m = 1955 + \Delta t_{m,3\sigma} = 2131$ y. The interval is estimated in Section A.5.

Comparison in Section 4 with the projections in Figure TS.4, page 53, of the Technical Summary in [4], which are obtained by complex/intermediate simulation packages, and are driven by business-as-usual and mitigation policies, shows that only the projection period close to the present complies with finite-reserve predictions, as already observed in [10] and [14]. The paper ends with a brief discussion and analysis of the issue, which takes advantage of the simple dynamic model of Section 2.

2 A Dynamic Model of the Carbon Dioxide Absorption by Land/Ocean Sinks

2.1 Model Variables and Notations

The aim of the section is to formulate a dynamic model of the annual mean carbon exchange, which excludes the seasonal carbon cycle (see [22]), but is capable of fitting the airborne CO_2 drift of the industrial era. Fossil-fuel emissions and their absorption by land and ocean sinks will be accounted for. To this end, it seems natural to define the reservoirs ('pools' is an alternative term) of Table 1, capable of storing an amount x_s of carbon dioxide under different forms. Something like this has been sketched in [21] and referred to as the "Carbon Cycle Orrery" (see [5, 6, 34–36], and [37]).

The simplified symbols of u_5 in rows 8 and 9, though denoting the same variable, are employed in different contexts: (i) $u(t) > 0$ denotes the CO_2 input flow of the state Eq. (10) and (ii) $-c(t) < 0$ denotes in (24) the CO_2 output flow of the fossil-fuel deposit.

To avoid symbol multiplication, instances of the same variable, say x, will be distinguished by marks as in Table 2. The most complicated mark applies to regression residuals where hat and tilde pile up. The column "Section" refers to the first Section of usage.

The reservoir state variables (briefly states or levels) are collected into the column vector $\boldsymbol{x} = [x_1, x_2, x_3, x_4, x_5]$, where the inline notation of [29] has been adopted. The term reservoir implies both CO_2 emission and uptake, whereas sink just indicates uptake and deposit emission.

In the proposed dynamic formulation, the amount $x_s(t)$, or the relevant chemical compounds, of each reservoir is a state variable, whose time rate equals a combination of input (positive) and output (negative) exchange flows $\pm v_{sh}(\boldsymbol{x}, \Theta)$ and of the anthropogenic flow $\pm u_s$. The exchange flows are assumed to depend on the reservoir levels and on the global temperature Θ at the boundary layers of atmosphere, land, and ocean. Detailed equations are derived in the Appendix and then simplified into a pair of state equations driven by the emission u_5 of the fuel combustion. The first equation

Table 2 Variable instances and their marks

No.	Variable instance	Symbol	Section	Variable instance	Symbol	Section
1	Error variable (tilde)	$\widetilde{x}$	2.3	Measurement (breve)	$\breve{x}$	2.2
2	Annual mean, constant value (overline)	$\overline{x}$	2.2	Equilibrium value (underline)	$\underline{x}$	1,2.1
3	Estimated variable (hat)	$\widehat{x}$	2.4	Regression residuals (tilde and hat)	$\widehat{\widetilde{x}}$	2.4
4	Time derivative	$\dot{x}$	1, 2.2	Time derivative of the mean	$\dot{\overline{x}}$	2.2

indexed by $s = 1$ and developed in this section expresses the annual mean concentration $x = x_1 = \left[CO_2\right]_{atm}$ of the airborne CO_2 as the combination of anthropogenic emissions and of the land/ocean absorption. The expression of the land/ocean absorption implicitly includes the effect of the carbon feedback [21], which the paper does not need to explicitly estimate. Subscript 1 will be dropped. The second equation, which is indexed by $s = 5$ and will be employed in Sect. 3, expresses the depletion of the fossil-fuel reserve level $r = x_5$.

In the next sub-sections, the equation indexed by $s = 1$ is derived by physical/chemical arguments, which provide a justification of the Appendix model. The equation is then converted into a perturbation equation around the unknown CO_2 equilibrium $\underline{x} = \underline{x}_1$ (underlining denotes equilibrium) and employed for fitting equation parameters to historical data.

2.2 Annual Mean Rate and Concentration: Definition and Units

The annual mean concentration $\bar{x}(t)$ of the atmospheric carbon dioxide, which excludes the zero-mean component of the seasonal carbon cycle, is defined by the integral

$$\bar{x}(t) = \frac{1}{T}\int_{t-T/2}^{t+T/2} x(\tau)d\tau \text{ [ppm]}, \; T = 1 \text{ y}, \tag{1}$$

where $x(t)$ denotes the current concentration in a given volume of the dry atmosphere, in parts per million [ppm], and the time t is given in fractions of year [y]. Here, annual mean values are overlined to distinguish them from current values, but the notation will be abandoned when unnecessary. The integer $t_0 = \text{floor}(t)$ corresponds to the time 0:0 of January 1. The current year is denoted by $t_i = t_0 + iT = t_0 + i, i = 0, 1, \ldots,$ where t_0 must be chosen. The generic time instant is defined as $t = t_0 + iT + \tau, 0 \le \tau < T = 1$. Since the mean $\bar{x}$ is measured from January to December, the corresponding sample $\bar{x}(i)$ is referred to the year mid time $s_i = t_i + T/2 = t_i + 1/2$, which leads to the notation $\bar{x}(i) = \bar{x}\left(s_i\right)$. The annual mean rate $\dot{\bar{x}}(t)$ can be proved to coincide with the increment:

$$\dot{\bar{x}}(t) = T^{-1}(x(t + T/2) - x(t - T/2))[\text{ppm/y}]. \tag{2}$$

Figure 1a shows the measurements of the mean CO_2 increment $X(i) = \breve{x}(i) - \breve{x}(0)$ (blue color, the "breve" mark denotes measurements, see Table 2, row 1) from the Scripps Research data record [26] since $t_0 = 1750$ y, and the measured cumulative sum $C(i) = T\sum_{k=0}^{i} \breve{c}\left(t_k\right)$[ppm] (red color) of the fossil fuel emissions [ppm/y] from GCP data. Measurements are in units of concentration [ppm] and concentration rate [ppm /y]. The natural measuring unit of the CO_2 amount (the state variable x_s) in the reservoir s would be a mass unit like billion of metric tons [$GtCO_2$], but the [ppm] unit will be usually employed. The conversion factor μ_{CO2} from CO_2 mass to concentration in the dry air is given by the following:

$$\mu_{CO2} = \frac{1}{m_{ppm}} = \frac{1}{7.804}\frac{\text{ppm}}{\text{GtCO}_2} \iff m_{ppm} = \frac{m_{dry\_air}}{10^6}\frac{M_{CO2}}{M_{dry\_air}}, \\ = \frac{5.135 \times 10^6 \text{ Gt}}{10^6}\frac{44.01 \text{ g/mol}}{28.96 \text{ g/mol}} \tag{3}$$

where the mean dry-air mass m_{dry_air} comes from [40], and M_{CO2} and M_{dry_air} are the molar masses of CO_2 and the dry air, respectively.

We distinguish between the measurement $\breve{x}(i)$ and the unknown "true" value $\bar{x}_{true}(i)$ of the global airborne CO_2 mean annual concentration. Their relation can be written as follows:

$$\breve{x}(i) = \bar{x}_{true}(i) + \delta x(i) + \tilde{x}(i) = \bar{x}(i) + \tilde{x}(i), \tag{4}$$

where $\delta x(i)$ is the unknown, but bounded, model error and $\tilde{x}(i)$ is the random measurement error. According to [19], $\delta x(i)$ is believed to be rather negligible due to the Mauna Loa Observatory privileged location, but nonetheless it exists and depends of the atmospheric volume definition. Investigation about $\delta x(i)$ is not a scope of the paper. Thus, the true value will be taken as $\bar{x}(i) = \bar{x}_{true}(i) + \delta x(i)$.

2.3 Derivation of the State Equation

The main reservoirs capable of absorbing airborne CO_2 are the ocean and land sinks. The reservoir in seawater can be explained by the seawater reactivity, which is alkaline in character. The equilibrium constant of the relevant reaction

$$CO_2(\text{gas}) + H_2O \iff CO_2(\text{aq}) + H_2O \iff H_2CO_3 \tag{5}$$

has been discussed in [21, 30, 31, 41], and [42].

The land sink can be mainly explained by the photosynthesis, which encompasses, in the very first stages, a reaction similar to (5) between carbon dioxide and water, that constitutes the cell cytoplasm. Carbon dioxide enters the cell through the cell membrane, where is incorporated into already existing organic carbon compounds. Using the organic compounds ATP (adenosine triphosphate, a source of energy) and NADPH (nicotinamide adenine dinucleotide phosphate, a reducing agent), the resulting compounds are then reduced and removed to form further carbohydrates, such as glucose. Being the reaction (5) the first common stage of both sinks, it can be incorporated into the same mathematical treatment. The reaction (5) must be considered from the kinetic point of view, as the paper interest lies in situations where chemical reactions have not yet reached their equilibrium conditions. This happens because each year billions of tons of carbon dioxide are emitted into the

atmosphere by burning fossil fuels, thereby disturbing the pre-industrial equilibrium. As in any kinetic-controlled reaction, the direct (from left to right) and inverse (from right to left) semi-reactions must be considered. However, if we assume that the concentration $[H_2CO_3]$ of carbonic acid in seawater and in cytoplasm remains constant, at least in the decade time span, the inverse semi-reaction has nearly a constant rate. Conditions of the assumption will be formulated in the Appendix. By accounting for the direct reaction in (5), we can write the following differential equations, which express the depletion of the airborne CO_2 and the reverse reaction of the land and ocean depletion:

$$\begin{aligned} v_{dir}(t) &= -k_{dir}\left[CO_2\right]_{atm}(t) \\ v_{inv}(t) &= \frac{d[H_2CO_3](t)}{dt} = k_{inv}\left[H_2CO_3\right](t) = \overline{v}_{inv} \end{aligned}. \tag{6}$$

The overline in the rightmost part of the second row in (6) denotes constancy. The total reaction rate results from the sum $v_{dir} + v_{inv}$, namely,

$$\frac{d\left[CO_2\right]_{atm}(t)}{dt} = v_{inv} + v_{dir} = \overline{v}_{inv} - k_{dir}\left[CO_2\right]_{atm}. \tag{7}$$

This is only a part of the process, because every year a certain known amount of anthropogenic CO_2 is emitted into the atmosphere, and the negative absorption feedback $-k_{dir}\left[CO_2\right]_{atm}$ is weakened by the carbon feedback (CF) k_{CF} as shown in the Appendix (see [34, 36, 37, 43]). In essence, the CO_2 exchange between land/ocean and atmosphere, expressed by the reaction rates in (6), depends on the boundary temperature and in turn, the temperature is affected by the airborne CO_2. Equation (7), when completed by the term $\frac{d[CO_2]_{anthr}}{dt}$ that accounts for the CO_2 emission rate, by the initial condition $\left[CO_2\right]_{atm}(t_0) = \left[CO_2\right]_{atm,0}$ and by the net feedback gain $k = k_{dir} - k_{CF} > 0$, becomes

$$\begin{aligned} &\frac{d\left[CO_2\right]_{atm}(t)}{dt} = \overline{v}_{inv} - k\left[CO_2\right]_{atm}(t) + \frac{d\left[CO_2\right]_{anthr}(t)}{dt} \\ &\left[CO_2\right]_{atm}(t_0) = \left[CO_2\right]_{atm,0}. \end{aligned} \tag{8}$$

Although $k_{dir} > 0$ is weakened by the carbon feedback gain $k_{CF} > 0$, the actual net gain remains positive, $k > 0$, as shown by the regression results in Section 2.5. Only the net gain k is estimated in the paper.

Equation (8) implies that the pre-industrial equilibrium $\underline{\left[CO_2\right]}_{atm}$ can be obtained by setting $\frac{d[CO_2]_{atm}(t)}{dt} = \frac{d[CO_2]_{anthr}(t)}{dt} = 0$, which provides the equilibrium formula:

$$\underline{\left[CO_2\right]}_{atm} = \frac{\overline{v}_{inv}}{k}, \tag{9}$$

where the equilibrium symbol is underlined. The previous identity, which derives from the constancy of $\overline{v}_{inv}$, is the key assumption of the first-order state Eq. (10). It corresponds to Assumption 5 of the Appendix, and it will be justified in Section A.5. An explicit account of its fluctuations postulates a higher-order dynamic model as explained in the Appendix.

Notation simplification with the help of the Appendix and of Eq. (9) allows (8) to be rewritten as follows:

$$\dot{x}(t) = -k\left(x(t) - \underline{x}\right) + u(t) + w_u(t),\ x\left(t_0\right) = x_0, \tag{10}$$

where w_u denotes minor input terms to be explained below and in the Appendix. The input $u(t)$ may be affected by a time delay τ_u with respect to x. As explained in Section 2.4, what matters is the reciprocal delay/lead times between the measurements of u and x. The times have been estimated to be well less than one year. The following notation identities apply to (10):

$$x(t) = \left[CO_2\right]_{atm}(t),\ u(t) = \frac{d\left[CO_2\right]_{anthr}(t)}{dt}. \tag{11}$$

Equation (10) depends on the unknown parameters $\underline{x}\left[\text{ppm}\right]$ and $k\left[1/\text{s}\right]$, to be estimated from historical data since 1850. We remark that $\underline{x}$ has the meaning of unknown pre-industrial equilibrium (before 1850), to be estimated as $\hat{\underline{x}}$ from historical data of the industrial era in Section 2.4. The assumption can be a posteriori checked by taking the average $\underline{x}_{hist}$ of the historical airborne CO_2 concentration data $\breve{x}\ (t_i), t_i < 1850$ y, as in Table 3, Section 2.5, and in Section 2.6. It looks viable that the absolute error $\left|\hat{\underline{x}} - \underline{x}_{hist}\right|$ may work as a validation criterion of (10) and of the model parameter estimates. A quite extensive check of $\hat{\underline{x}} \cong \underline{x}_{hist}$ is reported in Section 2.6.

Table 3 Difference and integral regressions since 1955

No.	Parameter	Symbol	Unit	Estimate	A-posteriori standard deviation
1	Kinetic constant	$\hat{k}$	1/y	0.019 (0.019)	0.0016
2	Time constant	$\hat{\tau}$	y	53 (52)	4.6
3	Equilibrium concentration	$\hat{\underline{x}}$	ppm	286 (286)	2.4
4	Historical equilibrium	$\underline{x}_{hist}$	ppm	280	3.0 (until 1850)
5	Residual RMS	$\hat{\widehat{\sigma}}_{\Delta x}$	ppm	0.35 (0.52)	$\log_{10}\left(1 - R^2_{int}\right) = -3.5$

For the scope of this paper, (10) must be rewritten in terms of the mean annual concentration $\overline{x}(t)$ defined in (1) and in terms of the mean annual rate $\overline{u}$ of $\left[CO_2\right]_{anthr}(t)$, which is defined according to (2). Thanks to linearity, integration and derivation commute, and thus (10) does not change in terms of the mean variables, which suggests to keep the same notations of Eq. (10), namely $x = \overline{x}$ and $u = \overline{u}$.

The main contributors to the anthropogenic emission $u(t)$ are fossil-fuel combustion and land-use change, say deforestation. While the former, denoted by $c = u_5$, will be forecast in Section 3 under the constraint of finite proven reserves, the same prediction cannot be applied to the latter, denoted by u_3. It is included in (10) by splitting the time profile as $u_3(t) = \overline{u}_3 + \widetilde{u}_3(t)$, where $\overline{u}_3$ is a constant term ($\overline{u}_3 = 0.56 \sim 0.64$ ppm/y depending on the average interval) and $\widetilde{u}_3(t)$ a zero-mean fluctuation (see Assumption 7 in the Appendix). The mean term $\overline{u}_3$ becomes part of the constant flow $\overline{v}_{inv}$ in Eqs. (8) and (9), thus contributing to the airborne carbon dioxide equilibrium $\underline{x}$ by $\frac{\overline{u}_3}{k} \cong 32.6$ ppm ($\cong 11\%$), whereas $\widetilde{u}_3(t)$ becomes a component of the input $w_u(t)$. Thus, either explicitly adding $\overline{u}_3$ to Eq. (10) or implicitly adding $\overline{u}_3$ through its contribution to $\underline{x}$ must be kept as equivalent.

A similar equation to (10) but referred to ocean is found in [44]. Other dynamic models can be found in [11] and [45]. They are somewhat different from the asymptotically stable Eq. (10), since they include a bounded-input-bounded-output unstable component (see [29]), and therefore cannot be employed for long-term predictions.

2.4 Discretization and Parameter Estimation

In order to employ the measurements $\left\{\breve{x}\ (i), \breve{u}\ (i)\right\}$, $i = 0, 1, ..., N-1$ of the mean values x and u, Eq. (10) is rewritten as follows:

$$\delta\dot{x}(t) = -k\delta x(t) + u(t) + w_u(t),\ \delta x\left(t_0\right) = \delta x_0,\ \delta x(t) = x(t) - \underline{x}, \tag{12}$$

and integrated in the time interval $\mathcal{S}(i) = \left\{t; s_i \le t < s_{i+1}\right\}$. Integration [29] provides the discrete-time equation:

$$\delta x(i+1) = exp(-kT)\delta x(i) + \int_{s_i}^{s_{i+1}} \exp\left(-k\left(s_{i+1} - \tau\right)\right) \left(u(\tau) + w_u(\tau)\right)d\tau,\ \delta x\left(t_0\right) = \delta x_0. \tag{13}$$

Equation (13) can be arranged into a difference form, by defining $\Delta x(i) = x(i+1) - x(i)$ and by solving the convolution integral under the simplifying assumptions that $kT \ll 1$ (to be a posteriori checked) and that $\left|1 - \frac{u(\tau)}{u(i)}\right| \ll 1$. By replacing x and u with their measurements, with a "breve" mark on the top (see Table 2 row 1), and by including w_u into the overall error $\Delta\widetilde{x}(i)$, the following *difference regression* equation is found:

$$\Delta\ \breve{x}\ \left(s_i\right) = -(1-a)\left(\breve{x}\ (i) - \underline{x}\right) + b(a)\ \breve{u}\ (i) + \Delta\widetilde{x}(i), \tag{14}$$

where error variables are marked on top by a tilde and equilibrium variables like $\underline{x}$ are underlined. The unknown pair to be estimated is $\left\{a, \underline{x}\right\}$. The equation notations are as follows:

$$a = \exp(-kT),\ b(a) = \frac{1 - \exp(-kT)}{k} = \frac{(1-a)T}{\log(1/a)}. \tag{15}$$

As already remarked, we should account for delay/lead times $\left\{n_x, n_u\right\}$ between measurements and model variables, written as $\breve{x}\ (i) = x\left(i - n_x\right) + \widetilde{x}(i)$ and $\breve{u}\ (i) = u\left(i - n_u\right) + \widetilde{u}(i)$. What matters is the difference $\Delta n = n_x - n_u$. The difference has been estimated in the range $|\Delta n| \le 0.25$y by a regression sequence of $\Delta\ \breve{x}\ (i + k/12)$, $|k| \le 12$ versus $\breve{u}\ (i)$ as in (14). Thus, the difference Δn has been set to zero and the relevant deviations included in the overall error $\Delta\widetilde{x}(i)$.

The estimated pair $\left\{\hat{\underline{x}}, \hat{a} = \exp\left(-\hat{k}T\right)\right\}$ of (14) has been checked by the following *integral regression* equation:

$$\breve{x}\ (i) = \underline{x} + a^i\left(\breve{x}\ (0) - \underline{x}\right) + b\sum_{k=1}^{i} a^{i-k}\ \breve{u}\ (k-1) + \widetilde{x}(i), \tag{16}$$

where the annual mean $\breve{x}\ (i)$ of the Mauna Loa data equals the discrete-time integration of (13) [29].

Under the assumption of a statistically independent, zero-mean and stationary error $\widetilde{x}(i)$, of a zero-mean and non-stationary emission error $\widetilde{u}(i)$, and of the approximations $1 - a \simeq kT \ll 1$ and $b(a) \simeq T = 1$, the overall error $\Delta\widetilde{x}(i)$ and the a priori variance, restricted to the measurement errors, can be approximated as follows:

$$\begin{aligned} &\Delta\widetilde{x}(i) \simeq \widetilde{x}(i+1) - \widetilde{x}(i) - T\widetilde{u}(i) \\ &\mathrm{var}\Delta\widetilde{x}(i) \simeq 2\mathrm{var}\widetilde{x} + T^2\mathrm{var}\widetilde{u}(i) = 2\sigma_1^2 + \left(T\rho_c\ \breve{u}\ (i)\right)^2 < 0.1 \end{aligned}. \tag{17}$$

The value $\sigma_1 \simeq 0.12$ ppm (1σ uncertainty) accompanies the NOAA (National Oceanic and Atmosphere Administration) data set of the Mauna Loa CO_2 concentration annual mean [46] and appears to be the upper bound of the same uncertainty from other sources like [25]. The value $\rho_c \simeq 0.05$ comes from the 2021 report of the Global Carbon Project [25], where the 1σ uncertainty of the global fossil CO_2 emissions has been assessed at 5% of the emission itself.

As a mutual check, Fig. 2 shows three kinds of regression residuals since $t_0 = 1955$ y: (i) the difference regression residual $\Delta\hat{\widetilde{x}}(i)$ of (14) (dark green), (ii) the integral residual $\hat{\widetilde{x}}(i)$ of (16) (pointwise green), and (iii) the cumulative residuals (solid cyan), which are obtained by integrating (14) with the

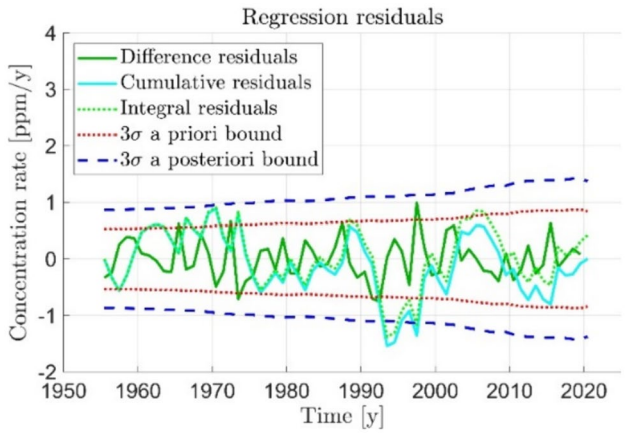

Fig. 2 Three kinds of regression residuals with a posteriori and a priori bounds

difference regression estimates. The regression residual, say $\widehat{\widetilde{x}}(i)$, marked by tilde and hat, plays the role of the estimate of the regression equation error $\widetilde{x}(i)$. The rate unit [ppm/y] in Fig. 2 would only apply to difference residuals. Actually, since the time unit is one year, integral and cumulative residuals [ppm] can be converted into rate units [ppm/y] without changing their values. Cumulative and integral residuals track each other with a small drift due to slightly different estimated values (see Table 3, Section 2.5). The integral residuals tend to be larger than the difference regression, because of the mid-frequency components of $w_u(t)$. For instance, the negative overshoot of the integral and cumulative residuals since 1990 is not fortuitous, but is mainly due to the Pinatubo volcanic eruption [47], which forced a short-term decrease of the CO_2 growth rate. Estimated residuals are compared with the 3σ a priori bound from (17) and with the residual a posteriori bound. The bounds increase because of the non-stationary error $\widetilde{u}$ in (17).

2.5 Regression Results

Difference and integral regression results are shown in Table 3 for $t_0 = 1955$ y. Annual mean data are available from the Scripps Research program [26] since $t_0 = 1750$ y, but the concentration rate data from ice cores (before 1959, [48]) look rather irregular as shown in Fig. 1b, which suggested to restrict regression from $t_0 = 1955$ y (the shaded area in Fig. 1b).

The regression results are summarized in Table 3 (integral regression estimates are in brackets). The estimated time constant $\widehat{\tau}$ refers to the absorption of the atmospheric CO_2 by the whole Earth sinks, mainly land and ocean. In other terms, all the absorption kinetic constants are summed up as in the entry (1,1) of the matrix A in (A.14). The small ratio $1 - R^2_{int}$ (in logarithmic scale, Table 3, last row), between the residual sum of squares and the total sum of squares of the integral regression, guarantees the model significance.

In Table 3, the a posteriori standard deviations $\widehat{\sigma}_x$ and $\widehat{\sigma}_\tau$ of the estimated parameters $\underline{\widehat{x}}$ and $\widehat{\tau} = \frac{1}{\widehat{k}}$ have been obtained by exploiting the quasi-linear regression in Eq. (14).

Literature estimates are rather sparse. In [44], the estimate for the ocean sink absorption amounts to 10 years. In [21], a value of 100 years is reported. The IPCC Working Group I, in [49], reports values from 5 to 200 years, by remarking that "No single lifetime can be defined for CO_2 because of the different rates of uptake by different removal processes." Other values are reported in [11]. The FAIR model in [50] describes the land/ocean CO_2 absorption as actuated by four parallel pools each associated with absorption time constants ranging from 4.3 years to 1 million years, the last value accounting for a geological absorption. In Section 2.7, the time constant estimate will be checked by rewriting a key equation of [34] and [37] in terms of (10).

Figure 3a shows the measured airborne CO_2 concentration rate $\Delta \breve{x}(i)$ (blue color) since 1955, the relevant estimated profile (dashed red) and the residual $\Delta\widehat{\widetilde{x}}(i)$. The residual short-term fluctuations may be partly explained by including, as a component of $w_u(t)$, the temperature anomaly of a Pacific Ocean equatorial belt, which is employed to monitor the El Niño phenomenon [47]. The residual RMS of the difference regression reduces to below 0.29 ppm (with a square reduction of about 35%). The scale factor sign is estimated to be positive, meaning that ocean absorption weakens with increasing temperature (in agreement with the carbon feedback effect). El Niño historical data cannot be long-term predicted, preventing their use in Section 3. Figure 3b shows the raw mean CO_2 concentration increment $\breve{x}(i) - \underline{\widehat{x}}$ (blue line) and the estimated profile (dashed red) with respect to the estimated pre-industrial equilibrium (the dashed zero line). Regression residuals are also shown.

2.6 Regression Extension to Whole Industrial Era

Regression restriction to the recent epoch since 1955 may rise questions about model and estimate validity and robustness versus longer periods of the industrial era. The criterion suggested in Section 2.3, namely the absolute error $\left|\underline{\widehat{x}} - \underline{x}_{hist}\right|$ of the equilibrium estimate, can be accompanied by the RMS of the regression residuals. Regression extension to industrial era should be deemed not necessary for future predictions, since as Fig. 1b shows, significant increment of fossil-fuel emissions just started around 1950. In [11] and [21], emissions until 1950 are mainly justified by deforestation. Aiming to check regression validity and robustness, a sequence of $M = 6$ difference regressions has been done from 1860 until 1960, with incipit dates equal to $t_0(k) = 1860 + 20k$ y, $k = 0, 1, ..., M - 1$.

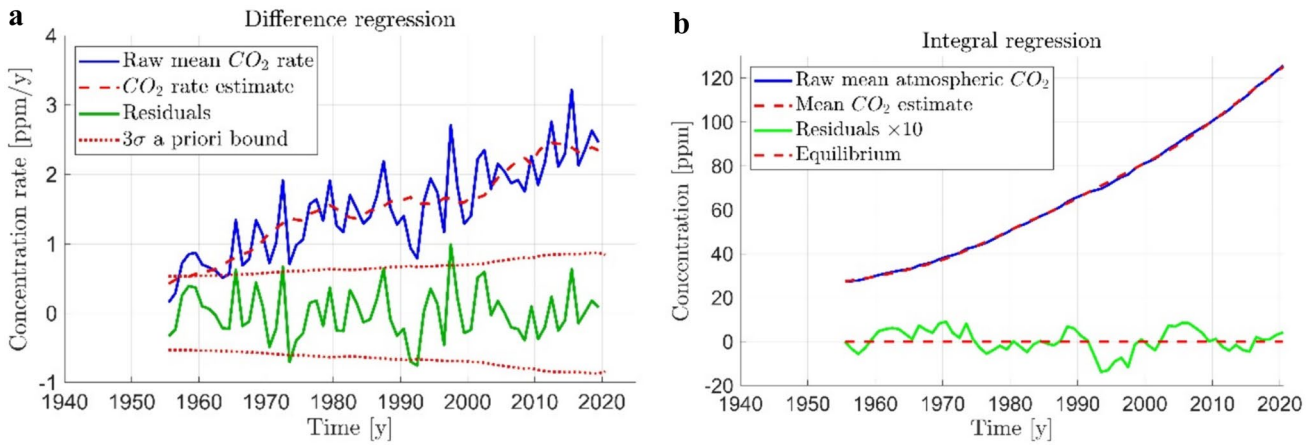

Fig. 3 **a** Mean annual airborne CO_2 concentration rate (from Scripps Research data [26]): estimate and residuals with 3σ a priori bound. Difference regression. **b** Mean annual airborne CO_2 concentration (from Scripps Research data [26]): estimate and residuals. Integral regression

Figure 4 shows the sequence of parameter estimates (blue and red lines) and their 3σ uncertainty band. The width of the uncertainty bands slightly increases toward earlier dates since it is partly compensated by a larger size of the measured samples. The small bias of the CO_2 equilibrium fractional error, namely $\left|\frac{\hat{\underline{x}}}{\underline{x}_{hist}} - 1\right| < 0.02 \sim 0.06$, though accompanied by the explosion of the integral residuals (dark green), can be taken as a validity and robustness check. The explosion occurs because of the integration of mid-frequency residual components, which also justifies the increase of $\left|\hat{\underline{x}} - \underline{x}_{hist}\right|$.

2.7 Comparison with Carbon Feedback Literature

Let us consider in [34] the key relation between the total airborne CO_2 increment $\Delta x(t) = x(t) - x(t_0)$ (including the carbon feedback perturbation) and the exogenous increment due to the input $U(t) = u(t) + w_u(t)$ in (10):

$$\Delta x(t) = \frac{1}{(1-g)(1+\beta)} \int_{t_0}^{t} U(\tau) d\tau,\ g = -\frac{\alpha\gamma}{1+\beta}. \tag{18}$$

Of the symbols $\{g, \alpha, \beta, \gamma\}$ from [34], α [K/ppm] is the global temperature sensitivity to airborne CO_2 and γ $[\frac{\text{ppm}}{\text{K}}]$ is the sensitivity of the land/ocean carbon uptake to global temperature. Equation (10), once integrated, becomes

$$\delta x(t) = h\left(\Delta t_x\right) \delta x\left(t_0\right) + \int_{t_0}^{t} h(t-\tau) U(\tau) d\tau, \tag{19}$$

with $\delta x(t) = x(t) - \underline{x}$, $\Delta t_x = t - t_0$ and $h\left(\Delta t_x\right) = \exp(-k\Delta t_x)$. The free response can be eliminated by assuming the initial state equal to the airborne CO_2 equilibrium, namely $x\left(t_0\right) = \underline{x}$, in which case $\delta x(t) = \Delta x(t)$. The input integral of

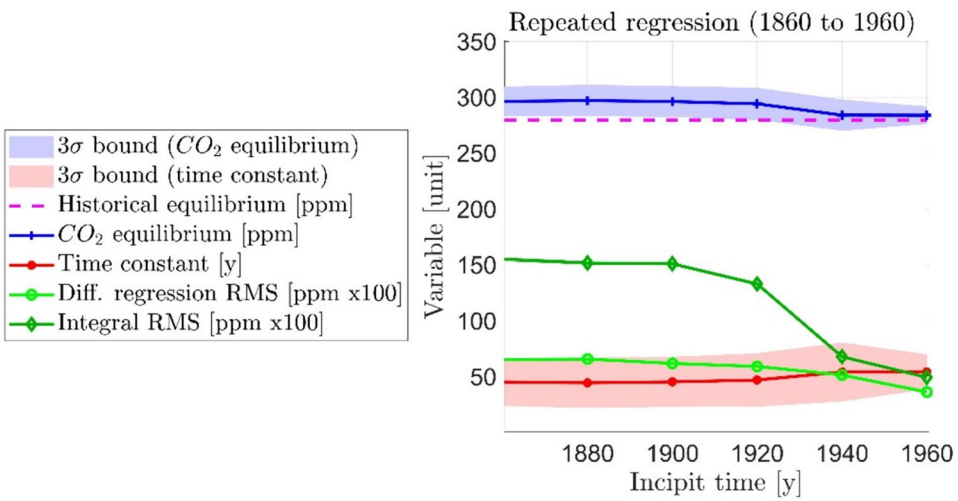

Fig. 4 Sequence of regressions: parameter estimates, uncertainty, and residuals

(18) can be introduced into (19) by assuming that $h(\Delta t_x)$ slowly decays like when $k\Delta t_x < 1$ and consequently by replacing $h(t-\tau)$ with the mean value $\frac{1}{\Delta t_x}\int_{t_0}^{t} h(t-\tau)d\tau = \frac{1-\exp(-k\Delta t_x)}{k\Delta t_x}$, thus leading to the approximation

$$\Delta x(t) \cong \frac{1-\exp\left(-k\Delta t_x\right)}{k\Delta t_x}\int_{t_0}^{t} U(\tau)d\tau. \tag{20}$$

The function $\frac{1-\exp(-x)}{x} \le 1$ is such that, for $x \ge 0$, one can find a monotonically decreasing function $\eta(\infty) = 1 \le \eta(x) \le \eta(0) = 2$, which satisfies the equality

$$\frac{1-\exp(-x)}{x} = \left(1+\frac{x}{\eta(x)}\right)^{-1}. \tag{21}$$

Use of the last identity, and replacement of k with $k_{dir} - k_{CF}$ as in (8), allows (20) to be rewritten as

$$\Delta x(t) \cong \frac{1}{\left(1-\frac{k_{CF}\Delta t_x/2}{1+k_{dir}\Delta t_x/2}\right)\left(1+\frac{k_{dir}\Delta t_x}{\eta}\right)}\int_{t_0}^{t} U(\tau)d\tau, \tag{22}$$

which is the same expression of (18) under the identities

$$g = \frac{k_{CF}\Delta t_x}{\eta + k_{dir}\Delta t_x},\ \beta = \frac{k_{dir}\Delta t_x}{\eta}. \tag{23}$$

The first identity shows that, under $k_{dir}\Delta t_x \gg \eta$, g is nothing else than the ratio between the carbon feedback correction k_{CF} and the land/ocean absorption kinetic constant k_{dir}.

The estimate $\widehat{\beta} \cong 1.52$ in [37] for the period 1880–2017, such that $\Delta t_x = 138$ y provides, by iterating the identity (21), $\eta\left(\widehat{k}_{dir}\Delta t_x\right) = 1.48$ and $\widehat{k}_{dir} \cong 0.0163\ \mathrm{y}^{-1}$, which is within the 2σ uncertainty interval of the estimate $\widehat{k} = 0.019 \pm 0.0032\ \mathrm{y}^{-1}$ (2σ) in Table 3, row 1. A coherent value $\widehat{\beta} \cong 1.67 \pm 0.56$ can be found in [43], but referred to 1750–2011. CO_2 emission and concentration growth before 1850 should be treated as negligible and highly uncertain (see Fig. 1a), which leads to $\Delta t_x = 161$ y. The resulting estimate $\widehat{k}_{dir} \cong 0.015 \pm 0.004\ \mathrm{y}^{-1}$ partly overlaps the uncertainty band of $\widehat{k}$.

3 Forecasting the Fuel CO_2 Emissions Under Finite-Reserve Constraint

3.1 Introduction and Scope

In order to employ Eq. (10) for forecasting the CO_2 concentration (Sect. 4), we need to predict the input signal $u(t), t \ge t_P$, which, as already said, is restricted to the fossil-fuel emission $c(t) = u_5(t)$. The time $t_P = 2021$ y is the starting epoch of the projection. Forecasting will be done by extending the historical fuel consumption $c\left(t_i\right), t_0 \le t_i < t_P$, by means of a parameterized analytic model: the skewed Meixner distribution (also known as skewed/generalized hyperbolic secant distribution, [38, 39]). Forecasting will be constrained by the available reserves, namely by the estimated amount $r\left(t_P\right)$ of the fossil-fuel deposits at the present date t_P, whose equation from the Appendix holds:

$$\dot{r}(t) = -c(t),\ r\left(t_P\right) = r_P. \tag{24}$$

To do this, fossil fuel consumption and reserves are split into three categories indicated by $f = 1, 2, 3$, namely coal ($f = 1$, lignite is included), oil ($f = 2$, shale oil is excluded), and natural gas ($f = 3$, shale gas is excluded). The total predicted emission until the zero-reserve date t_{End}, namely

$$\widehat{c}\left(t_i\right) = \sum\nolimits_{f=1}^{3}\widehat{c}_f\left(t_i\right), i = N, N+1, ..., N+M-1,$$
$$t_N = t_P, t_{N+M-1} = t_{End} \tag{25}$$

will be employed in (10) to predict the airborne CO_2 concentration $\widehat{x}\left(t_i\right)$.

3.2 Reserves and Resources

In order to quantify the amount of fossil fuels left for use, let us distinguish between reserves and resources [51]. Resource is that amount of a natural commodity that exists in both discovered and undiscovered deposits. Reserves are that subgroup of a resource that have been discovered, that have a known size, and that can be technically recovered at a cost that is financially feasible at the present price of that feedstock. As a consequence, the known reserves of fossil fuels vary in time, with an increasing trend in the last decades, as shown in Fig. 5a, whose raw data (solid lines) are provided by OWID (Our World In Data) [52].

Let us denote the reserve amount of a generic fossil fuel with $r(t)$. By supposing that the trend of the raw data in Fig. 5a will attain a constant value r_∞ in the years to come, the trend can be predicted upon knowing the diminishing law of the future marginal reserves $m(t) = r_\infty - r(t)$ with initial condition $m_0 = r_\infty - r_0$ at time $t = t_0$. A law of this kind is usually arranged by assuming the relative variation $d\log m(t)$ to be proportional (with negative sign) to the dimensionless time interval $ds(t) = \frac{dt}{\tau}$ as follows:

$$d\log m(t) = -ns(t)^{n-1}ds(t),\ m\left(t_0\right) = m_0,\ s(t) = \frac{t-t_0}{\tau}. \tag{26}$$

The range $1 < n < 2$ is assumed for compelling the decrement to be slightly faster than the exponential, thus accounting for increasing difficulties in finding new reserves. Integration of (26) provides the explicit law:

$$r(t) = r_\infty - m_0\exp(-s(t)^n),\ t \ge t_0. \tag{27}$$

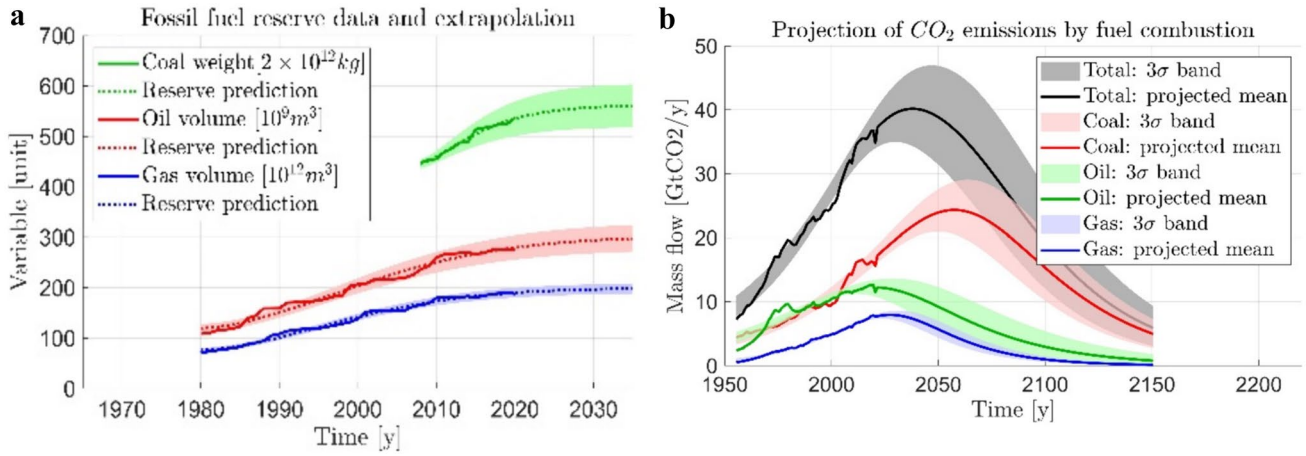

Fig. 5 **a** Raw data from OWID [52] and projection of fossil-fuel reserves (mass and volume units), together with 3σ uncertainty bands (the shaded areas). **b** Projection of the mean CO_2 emissions by fuel and of their total (mass flow in [$GtCO_2$/y]) together with 3σ uncertainty bands (the shaded areas)

The asymptotic value r_∞ defines the ultimate reserve value, to be used for further analysis. The parameters $\{\tau, m_0, r_\infty, n\}$ are found by fitting the raw data in Fig. 5a (solid lines); they vary with the fuel category f. Given the parameter estimates, the reserve $r(t)$ in (27) can be projected to future dates as in Fig. 5a (dashed lines). The shaded bands around the predicted curve $r(t)$ correspond to 3σ uncertainty. The estimated $r_{\infty,f}$ of the fuel ultimate reserve in Table 4, column 3, looks rather close to the 2010 estimates in [16].

We have now to determine which amount of carbon dioxide will be emitted in their future combustion until depletion is reached. Chemically speaking, the mass of carbon dioxide, produced by a unitary fuel mass, can be inferred from the fuel chemical composition by balancing simple chemical reactions. However, since chemical composition of fuels (coal and oil) is far from being expressed by a single chemical compound, another way has been adopted. OWID datasets about fossil fuels [52] reports the annual consumption of each fuel category during the 1980–2020 period, and the relevant emissions. Data elaboration provided the estimate of the conversion factor ρ_f as the mean annual emitted CO_2 mass of the fuel unit mass. The CO_2 equivalent ultimate reserve of the fuel f is denoted by $R_f = \rho_f r_{\infty,f}$. Values are in Table 4, column 5, together with the estimates in [11] (2007, column 6) and [16] (2010, column 3, in brackets).

3.3 Fossil-Fuel Emission Projection

Given historical fossil-fuel emissions, the aim is to predict the future by accounting for the finite reserves in Table 4. Let us denote the cumulative consumption of the fossil fuel f, in equivalent CO_2 mass units [$GtCO_2$], by $C_f(t_i) = \sum_{k=N}^{N+i} c_f(t_k)$, and let us assume that the future cumulative consumption equals the reserve amount R_f, that is $C_f(t_{End}) = R_f$.

The future interval starts from the end of the historical data, $t_P = 2021$ y, and expires at $t_{End} = 2150$ y, which, as already mentioned at the end of Introduction, has been chosen to comply with the model validity interval (see Section A.5) and to allow depletion of the large coal reserves. Oil and natural gas projections appear as rather invariant to $t_{End} > 2100$, being depleted just after this date (see Fig. 5b). The total (all the fuel categories) cumulative emission is denoted by $C(t_i)$ and the annual emission by $c(t_i)$ [$GtCO_2$/y]. The emission $c_f(t_i)$ of each category is approximated and predicted by an analytic function $c_f(t) = g(t; \boldsymbol{p}_f)$ depending on the parameter vector $\boldsymbol{p}_f$ to be estimated from historical data. The symmetric logistic curve has been employed in [11] and [14]. The chosen prediction curve is the four-parameter skewed Meixner distribution, whose shape recalls an asymmetric bell. The reasons for its choice are simplicity and being the product of three expected and significant terms: amplitude a, bell shape $\frac{1}{\cosh(\sigma)}$ and skew-

Table 4 Predicted reserve and equivalent CO_2 emissions

No	Fuel	$r_{\infty,f}$ from (27) (in [16])	Unit	R_f [$GtCO_2$]	R_f [$GtCO_2$] in [11]
1	Coal	1100 ± 30 (1σ)(1000)	10^{12}kg	$2100 \pm 95(1\sigma)$	1500
2	Oil	300 ± 8 (1σ)(210)	$10^9 m^3$	$690 \pm 54(1\sigma)$	500
3	Gas	200 ± 3 (1σ)(190)	$10^{12} m^3$	$370 \pm 19(1\sigma)$	350

ness $\exp(\beta\sigma)$. Their product, free of the subscript f, is written as follows:

$$g(t;\boldsymbol{p}) = a\frac{\exp(\beta\sigma)}{\cosh(\sigma)}, \sigma = \frac{t-s}{\tau}, \quad \boldsymbol{p} = [a, \beta, \tau, s]. \tag{28}$$

The meaning of the four parameters is as follows: $a = \max_t g(t)$ (the height of the maximum under $\beta = 0$) is the scale factor, $s = \arg\max_t g(t)$ denotes location (the abscissa of the maximum under $\beta = 0$), τ defines the bell width and $-1 < \beta < 1$ defines the skewness degree. The degree β tends to become unidentifiable when the measurements are restricted to a lobe of the bell (either left or right), that is either to $\sigma(t_k) < 0$ or $\sigma(t_k) > 0$. The former is the present case, which suggests the adoption of the symmetric shape with $\beta = 0$. Nonetheless, the paper projections look compatible with those in the literature under the assumption of finite reserves (see [10–12], and [16]). In fact, the left lobe happens to be dominated by raw data. The reserve bound is completed by constraining the final emission to approach a small value $\breve{c}_{End}$. As a sensitivity result, by lessening the pair $\left\{\breve{c}_{f,End}, t_{End}\right\}$, the bell width shrinks, and the emission peak $c_{f,max}$ grows up, whereas the opposite occurs by increasing the pair. The negative sensitivity $\Delta c_{max}/\Delta t_{End}$ of the fuel emission peak c_{max} with respect to t_{End} is reported in Table 5, Section 4.1, as "mean peak rate".

Given the emission measurement $\breve{c}_f(t_k)$ and the reserve estimate R_f, the regression equations read as follows:

$$\begin{aligned} \breve{c}_f(t_k) &= g(t_k;\boldsymbol{p}_f) + \tilde{c}_f(t_k), k = 0, \ldots, N-1 \\ R_f &= \textstyle\sum_{k=N}^{N+M-1} g(t_k;\boldsymbol{p}_f) + \tilde{R}_f \\ \breve{c}_{f,End} &= g(t_{End};\boldsymbol{p}_f) + \tilde{c}_f(t_{End}) \end{aligned} \quad . \tag{29}$$

The first equation expresses the analytic model of the annual emission; the second equation constrains the projected cumulative emission to match the reserve R_f after conversion into equivalent CO_2 mass; the third equation forces the ultimate emission to approach zero. The regression criterion to be minimized is the weighted sum of the square errors in (29), the weights being proportional to the a priori variance of the measurements.

Figure 5b, Section 3.2, shows the projected emission profiles [$GtCO_2$/y] by fuel, based on historical data from 1955 to 2020 (the irregular part of the mean profile, central solid line). The shaded bands account for the uncertainty of the parameter vector $\hat{\boldsymbol{p}}_f$ and of the reserve R_f. The uncertainty band around the estimated profile of the historical data is smaller than the band around the projected profiles, since the former is poorly affected by the reserve uncertainty.

4 Airborne CO_2 Concentration Projection: Comparison and Discussion

4.1 The Projections of the Total Fuel Emission and of the CO_2 Concentration

The historical and projected total fuel emission $c(t) = \sum_{f=1}^{3} c_f(t)$ is shown in Fig. 5b (black curve) together with the 3σ uncertainty band.

The annual airborne CO_2 concentration $x(t)$ is projected until t_{End} by integrating Eq. (10) under the input $u(t) = c(t), t_P \le t \le t_{End}$. The mean profile and the 3σ lower and upper profiles of the airborne concentration are provided. The mean projection derives from the mean emission profile in Fig. 5b, and the pair $\{\hat{\tau}, \hat{\underline{x}}\}$ from Table 3, column 5. The 3σ lower and upper bounds derive from the 3σ emission profiles in Fig. 5b and from the 3σ parameter estimates $\{\hat{\tau} \pm 3\hat{\sigma}_\tau, \hat{\underline{x}} \pm 3\hat{\sigma}_x\}$. The positive sign applies to the upper bound and the negative to the lower bound.

The resulting mean profile and the 3σ uncertainty band of the projected concentration are reported in Fig. 6a. The dashed red line, which overlaps the mean profile until $t_P = 2021$ y, corresponds to the annual mean of the Mauna Loa measurements in Fig. 3b. The peak delay $\Delta t_{max} = t_{x,max} - t_{c,max}$ is coherent, as shown in Table 5, below, with the estimated time constant $\hat{\tau}$ of Eq. (10), if a duration $\Delta t_c \cong 220$ y of the fuel emission wave is guessed, as follows:

$$\Delta t_{max} \cong \frac{\Delta t_c}{2\pi}\tan^{-1}\left(\frac{2\pi\hat{\tau}}{\Delta t_c}\right) \cong 35 \text{ y}. \tag{30}$$

Table 5 Peaks and dates of the projected CO_2 emission and of the airborne concentration

No.	Variable	Parameter	Symbol	Unit	Range	From [14]
1	Concentration	Peak	x_{max}	ppm	450 ~ 550 (±10%)	≈ 480 ~ 560
2	Concentration	Mean peak rate	$\frac{\Delta x_{max}}{\Delta t_{End}}$	ppm/y	-1.0	NA
3	Concentration	Date	$t_{x,max}$	y	2064 ~ 2086	≈ 2080
4	Emission	Peak	c_{max}	$GtCO_2$/y	35 ~ 47	≈ 33 ~ 55
5	Emission	Mean peak rate	$\frac{\Delta c_{max}}{\Delta t_{End}}$	$GtCO_2/y^2$	-0.24	NA
6	Emission	Date	$t_{c,max}$	y	2030 ~ 2047	≈ 2030 ~ 2050
7	Concentration	Delay	Δt_{max}	y	34 ~ 39	≈ 30 ~ 50

The ranges of the projected concentration peak x_{max} and of the date t_{max} are summarized in Table 5. In addition, the mean peak rate of the projected concentration and emission, and the concentration delay Δt_{max} are reported. The mean peak rate is the sensitivity of the peak values x_{max} and c_{max} to change of the end time t_{End}.

4.2 Comparison with the Literature Projections and Discussion

Comparison with the literature requires some care, as projections in [3, 6, 53], and [54] concern the CO_2 equivalent of the whole atmospheric GHGs, which, as already noticed, follow different intake and removal mechanisms. Projections restricted to CO_2 appear in Figure TS.4, page 53, of the Technical Summary in [4].

A pair of roads are followed. Let us start by comparing the CAT projections of the equivalent CO_2 emissions by greenhouse gases, as in Fig. 6b, whose data are available. Since the projections in Fig. 5b are restricted to fossil fuels, the graphical comparison in Fig. 6b has been improved by downshifting the CAT current policy projections (solid and dashed red lines) in order to overlap the uncertainty band (the shaded area) of the paper projections. According to the OWID data, the constant down shift amounts to about $\Delta u = 13\,\mathrm{GtCO_2/y}$, which matches the sum of methane and nitrous oxide emissions converted into the CO_2 equivalent mass flow. A confirmation is given by the historical emission data (the red and blue irregular curves) which overlap less a small drift. The overlap confirms that the current policy scenarios (upper and lower) fairly coincide with the finite reserve scenario of this paper. Figure 6a shows also the projection of a climate mitigation policy, the "2030 targets."

The second set of comparisons addresses the recent IPCC projections in Figure TS.4, page 53, of the Technical Summary in [4], whose data are summarized in the Tables of [55]. They supersede previous IPCC and literature projections, like those in [8] and [15]. The dataset of the CO2 emission projections from 2015 to 2100, to be shown in Fig. 7 with the unit of concentration rate [ppm/y], has been found in the IIASA website (International Institute for Applied Systems Analysis, [56]). The data set of the CO_2 concentration projections from 2015 to 2500, to be shown in Fig. 8 until 2150, was found in the University of Melbourne website. The projections have been made with an updated version of the MAGICC model, maintained at the Climate & Energy College of the University of Melbourne [57].

Figure 7 compares the projection of the total CO_2 emission by fossil fuels in Fig. 5b with the IPCC projections (from the sixth Assessment Report, retrieved from [56]) of five different Shared Socioeconomic Pathways (SSP). To allow a better comparison with IPCC profiles, the mean CO_2 emission profile of the paper (dashed blue) has been added with the constant value $\overline{u}_3 = 0.62$ ppm of the land use emission (see the end of Section 2.3). As a result, the paper profile (line 6) accurately matches the SSP 2–4.5 profile (line 3) up to the 2060 year. Of course, a correct integration of the augmented emission $u_a(t) = u(t) + \overline{u}_3$ through Eq. (10) requires the new equilibrium $\underline{x}_a = \underline{x} - \overline{u}_3/k$ and implies that the projection of the land-use change emission remains constant and equal to $\overline{u}_3$.

The five scenarios are explained in [3] (see also [56]). SSPx-y.y stands for Shared Socioeconomic Pathway, x = 1 to 5 denotes the class of the scenarios, and y.y denotes the net radiative forcing [W/m^2] at year 2100. Radiative forcing is the name given by IPCC to the algebraic sum of natural (sun radiation change) and anthropogenic (GHG concentration change) exogenous radiant energy fluxes [W/m^2], which perturb the energy equilibrium of the Earth's biosphere and consequently the climate.

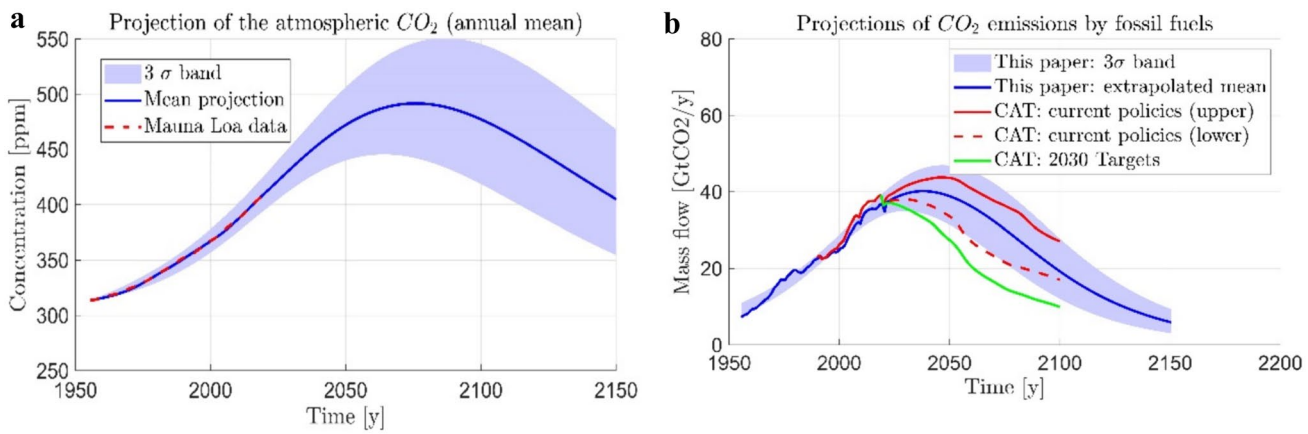

Fig. 6 **a** Projection of the atmospheric CO_2 concentration [ppm] based on Eq. (10) and on the estimated fossil-fuel reserves. **b** Comparison of the CO_2 emission projections (mass flow in [$GtCO_2$/y]) with the CAT projections [3], to which a downshift has been applied

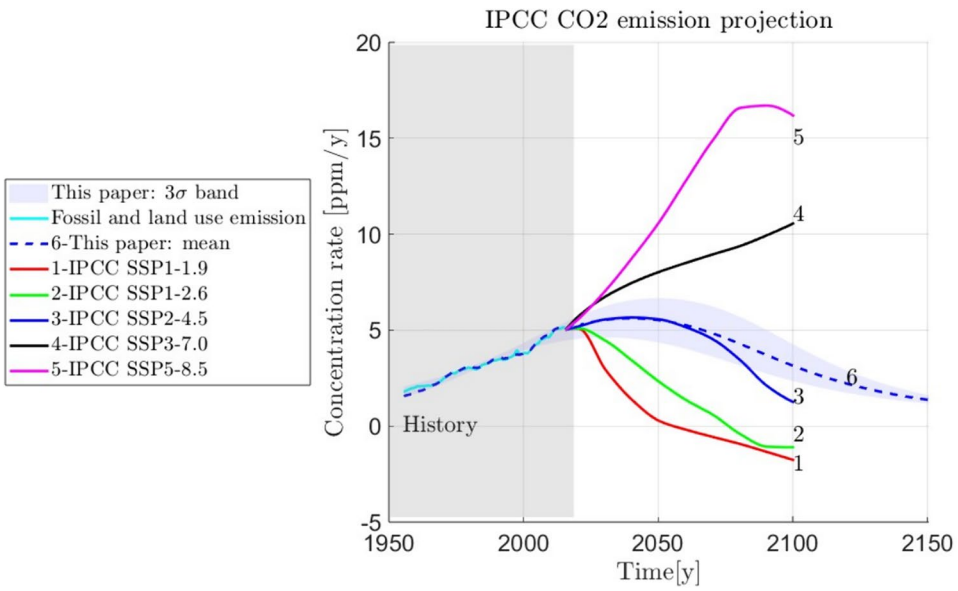

Fig. 7 Comparison of IPCC projections of CO_2 emissions (from IIASA dataset [56]) with the finite-reserve projections of this paper

The SSP 3–7.0 projection (line 4 in Fig. 7) assumes high GHG emissions and CO_2 emissions doubled by 2100. The SSP 5–8.5 projection (line 5 in Fig. 7) assumes very high GHG emissions and CO_2 emissions tripled by 2075. They look outside of the envelope defined by the finite-reserve projections of the paper. The SSP 2–4.5 projection (line 3 in Fig. 7) assumes intermediate GHG emissions and CO_2 emissions around current levels until 2050. Since then, it falls down but do not reach net zero emissions by 2100. The projection looks close to the mid profile of the CAT current policy projections in Fig. 6b and overlaps the mean finite-reserve projection of the paper (line 6 in Fig. 7). A similar conclusion was reached by [10] in the regards of the RCP (Representative Concentration Pathway) 4.5 in [15].

Figure 8 shows the comparison of the IPCC projections of the airborne CO_2 concentration, due to emissions in Fig. 7, with the finite-reserve projections in Fig. 6a. The cause-effect relation between IPCC profiles of Fig. 7 and Fig. 8 is suggested in the main page ("Greenhouse gas factsheets") of the University of Melbourne website. At first sight, comparison looks coherent with Fig. 7 in the sense that SSP 3–7.0 and SSP 5–8.5 projections (lines 4 and 5 in Fig. 8) lie outside of the envelope defined by finite-reserve projections.

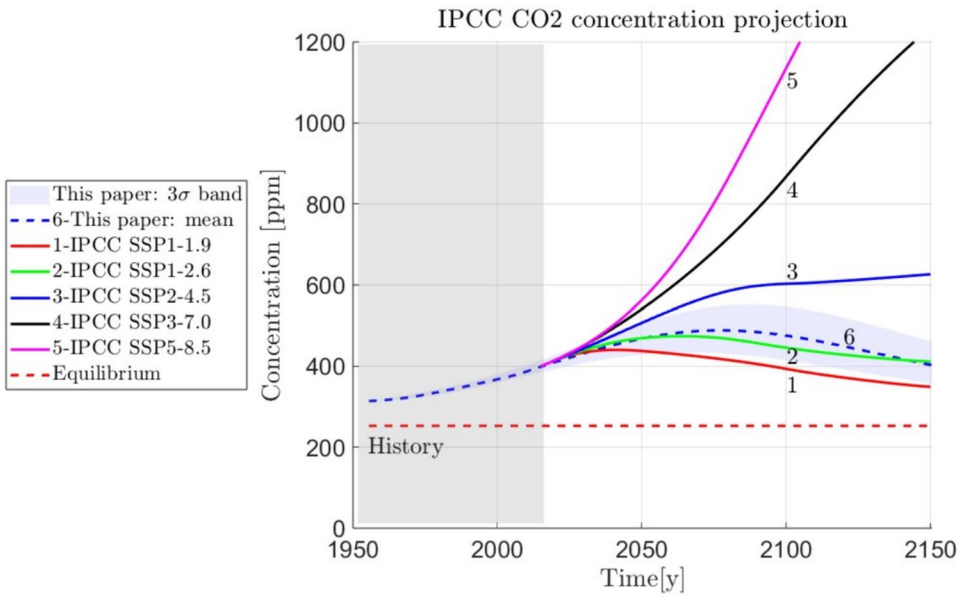

Fig. 8 Comparison of IPCC projections [57] of the airborne CO_2 concentration with the finite-reserve projections of this paper

However, the SSP 2–4.5 projection (line 3 in Fig. 8) significantly drifts away from the mean profile of this paper (line 6 in Fig. 8), notwithstanding the relevant CO_2 emission profiles (lines 3 and 6) overlap in Fig. 7. The drift deserves a better insight based on Eq. (10) and the parameters in Table 3. Integration of the SSP 2–4.5 emission profile through Eq. (10) should provide a similar shape as the dashed line 6 of Fig. 8, which is completely different from the SSP 2–4.5 concentration profile (line 3) in the same Figure. The increasing drift in the presence of a sustained emission reduction after 2050 y, would mean, in terms of Eq. (10), that the land/ocean absorption rate $-k(x(t) - \underline{x})$ progressively reduces to balance the residual emission $u(t) + w(t)$, which is impossible due to $x(t) > \underline{x} \cong 285$ ppm. The balance could be recovered by forcing either $k = \tau^{-1}$ to decrease (the time constant would increase above 50 y) and/or by forcing the equilibrium $\underline{x}$ to approach the current $x(t)$. Both remedies, which would be outside of the model assumptions, as formally given in the Appendix, embody the limits of the paper model and results.

The model captures the experimental mean annual exchange between atmosphere and the aggregated land and ocean and propagates to the future by assuming model parameter invariance, thus for instance neglecting their change due to near-surface temperature and airborne CO_2 concentration. Of course, we could force model parameters to vary in time, which has been done by accurately tracking the drifting profile 3 in Fig. 8 (see the MATLAB Live Script cited in the Data Availability). The findings must be kept outside of the paper scope, as the relevant time-varying mechanism was heuristic and unfit to experimental data. The authors expect, and it is the scope of the ongoing [58] and future work that a more complex model, as in the Appendix, endowed with a time-varying mechanism which is tuned on experimental data, may explain and validate the profiles of Fig. 8. The carbon cycle model of the MAGICC code [33], which produced the profiles of Fig. 8, and that of the FAIR model [50], should belong to this category.

As a final remark, we address the short interval (1955 to 2020) of the regression measurements, being of the same order of magnitude of the estimated time constant $\widehat{\tau}$. Firstly, the short-time duration of measurements reflects into the estimate uncertainty as in Table 3. Secondly, extension to longer past intervals as in Fig. 4 has shown rather invariant estimates. Thirdly, a confirmation comes from [37] and [43], as shown in Section 2.7. As a further concern, strictly related to time-varying mechanisms, one should address the time constant variability due to atmosphere, ocean, and land conditions, like the carbon feedback, whose growth is such to diminish the land–ocean absorption rate. For instance, the kinetic constant k in (10) and other parameters may include scaled perturbations driven by measurable and predictable exogenous variables, as in the FAIR model [50].

5 Conclusions

The paper starts from two observations: (1) the atmospheric CO_2 concentration growth rate is smaller than that ascribed to the emission of fossil-fuel combustion and (2) the fossil-fuel reserves are finite. The first observation leads to a simple and time-invariant state equation capable of accounting for the atmospheric CO_2 absorption by land and ocean, treated as an aggregate. The second observation leads to a simple bell-shaped curve for forecasting the emission of fossil fuels under current reserve constraint. Driving the state equation by the projected emission has allowed the airborne CO_2 concentration to be projected close to the zero-reserve epoch. In principle, the resulting mean profile and the relevant statistical bounds may be taken as upper physical limits to the projections of other scenarios.

The method advantage is rooted on simple physical models, whose parameters, being assumed time-invariant, can be estimated and checked from historical data, together with their uncertainty. Integration and estimation procedures can be easily repeated, checked, and updated. The projections of the fossil-fuel emissions have been derived by explicitly constraining them by proven reserves. Extension to GHG emissions from non-fossil sources was not the aim. Comparison with recent IPCC profiles of CO_2 emissions confirms that the 3σ range of the finite-reserve projections overlaps those of a moderate socioeconomic scenario like SSP2-4.5, in agreement with other authors. The comparison with the IPCC projections of the airborne CO_2 concentrations has revealed itself more complex, yet instructive, in view of model and method extension. The focus has been on the CO_2 airborne concentration (up to 2150 y), which is driven by SSP2-4.5 emissions. A significant mismatch has been found, in the sense that the relevant IPCC projection shows a sustained increase in the presence of a marked emission reduction (a decrease occurs only after the limit time of the assessment). The finite-reserve concentration, too, postpones the decreasing leg after the emission, but in a predictable way, which has been estimated in the paper.

The main reason of the mismatch that emerges from MAGICC and FAIR models is two-fold: (i) The dynamics of the global carbon cycle includes longer time constants than that estimated in the paper, and (ii) they change in time because of explicit/implicit time-varying mechanisms driven by perturbations of the temperature and CO_2 concentration. The relevant parameters appear tuned on the predictions of complex simulated models, unlike the simple model of the paper.

Ongoing and future research aims to the following: (i) complete the simple carbon dynamics of the paper with temperature dynamics and interconnections, as already mentioned in the Appendix; (ii) include other GHGs emissions,

not constrained by finite reserves, in the future projections; (iii) revise the Appendix model in the light of the literature; (iv) identify the proper land and ocean kinetic constants of the Appendix model, with the help of historical data; and (v) study and develop control strategies for the energy apportionment, capable of aiding a progressive reduction of fossil-fuel combustion under the energy demand.

Appendix

Derivation of state equations

A.1. Notations and Assumptions

Figure 9 sketches CO_2 reservoirs (pools in [50]) and flows. Earth's atmosphere is treated as a reservoir as well as fossil fuel deposits. Earth's interior as well as artificial reservoirs capable of capturing CO_2 are neglected. Main notations can be found in Table 1, Section 2.1. All the variables are assumed to be current annual averages as in (1) and their rates to be mean annual rates as in (2).

Given a time instant t, the existing concentration of CO_2 in the reservoir s is denoted by $x_s(t)$[ppm] and the time rate (uptake if positive or emission if negative) by $\dot{x}_s(t)$[ppm/y]. The sum $x_0(t) = \sum_{s=1}^{5} x_s(t)$ stands for the CO_2 amount in the Earth's biosphere at time t, which, by neglecting volcanic eruptions, is constant in time and implies the following assumption:

$$\text{Assumption 1} : \dot{x}_0(t) = 0 \text{ at any } t \geq t_0. \tag{A. 1}$$

Assumption 1 entrains that the time variation of the state $x_s(t), s = 1, ..., 5$ is only driven by CO_2 exchanges.

Two kinds of exchange rates, natural and anthropogenic, are distinguished. Natural emission from reservoir s to reservoir h, where CO_2 is absorbed, is denoted by $\pm v_{sh}\big(x_s(t), \Theta(t)\big)$, Θ being the global temperature [K] at the boundary between atmosphere and land/ocean surface. Negative sign refers to emission, positive sign to uptake. The series expansion of the exchange function around the constant equilibrium pair $\{\underline{x}_s, \underline{\Theta}\}$ is truncated to the first-order as follows:

$$\begin{gathered} v_{sh}\big(x_s, \Theta\big) \simeq v_{sh}\big(\underline{x}_s, \underline{\Theta}\big) + k_{sh}\delta x_s(t) + g_{sh}\delta\Theta(t)[\text{ppm/y}] \\ \delta x_s(t) = x_s(t) - \underline{x}_s\big[\text{ppm}\big], \delta\Theta(t) = \Theta(t) - \underline{\Theta}\ [\text{K}] \end{gathered} . \tag{A. 2}$$

In (A.2), k_{sh} is the kinetic constant [y^{-1}] of the exchange around the equilibrium $\underline{x}_s$, and g_{sh} [ppm/(y×K)] denotes the exchange thermal sensitivity. The first part of the first-order term has the same form of the direct and reverse reaction rates in (6), if $\big[CO_2\big]$ is interpreted as a perturbation from equilibrium.

The annual zero-mean two-way component of the natural exchanges (the biomass carbon cycle) is neglected by treating $x_s(t)$ as the current annual average of the reservoir levels as in (1). The following assumption is made:

$$\begin{gathered} \text{Assumption 2. Anthropogenic exchange only occurs} \\ \text{between reservoirs } s \neq 1 \text{ and } s = 1. \end{gathered} . \tag{A. 3}$$

The algebraic sum of emissions from and uptakes by $s \neq 1$ is denoted by $-u_s(t)$, negative when emission dominates. Anthropogenic emissions may account for exchange perturbations due to reduction and growth of reservoir capacity. For instance, land-use change may diminish land capacity, and the CO_2 uptake rate.

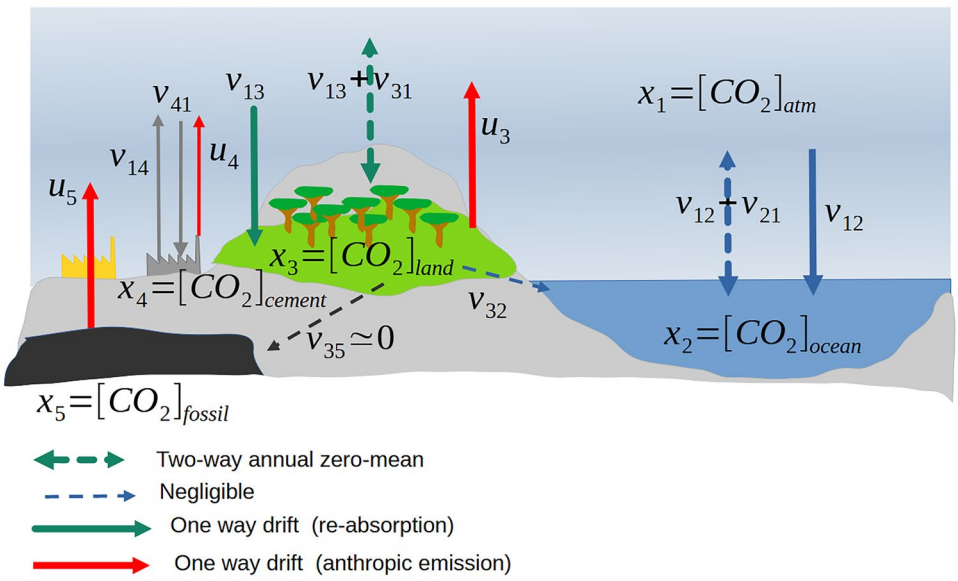

Fig. 9 Sketch of the main CO_2 reservoirs and their exchanges

A.2. The Carbon Feedback Identity

The global mean temperature dynamics is that of the single blackbody thermodynamics (also zero-dimension energy balance model), which for our scopes can be written as follows:

$$\dot{\Theta}(t) = F(\Theta(t), x(t), u(t)), \Theta\left(t_0\right) = \Theta_0, \tag{A. 4}$$

where $x(t) = x_1(t)$ is the airborne CO_2 concentration [ppm] and $u(t)$ accounts for exogenous sources [K/y]. The perturbation (also anomaly) equation around the recent Holocene equilibrium defined by $F\left(\underline{\Theta}, \underline{x}, \underline{u}\right) = 0$ reads as follows:

$$\delta\dot{\Theta}(t) = -f_\Theta \delta\Theta(t) + f_x \delta x(t) + f_u \delta u(t), \delta\Theta\left(t_0\right) = \delta\Theta_0, \tag{A. 5}$$

where $f_\Theta = \frac{\partial F\left(\underline{\Theta}, \underline{x}, \underline{u}\right)}{\partial \Theta} > 0\ [\mathrm{y}^{-1}]$ is a stabilizing feedback gain, $f_x = \frac{\partial F\left(\underline{\Theta}, \underline{x}, \underline{u}\right)}{\partial x} > 0\ [\mathrm{K/(y \times ppm)}]$ is the thermal rate sensitivity to CO_2, and the dimensionless $f_u = \frac{\partial F\left(\underline{\Theta}, \underline{x}, \underline{u}\right)}{\partial u}$ is the input gain. For our scope, Eq. (A.6) is rewritten by solving for $\delta\Theta(t)$ as follows:

$$\begin{aligned}\delta\Theta(t) &= \varphi_x \delta x(t) + \delta\underline{\Theta} + \delta\widetilde{\Theta}(t),\ \delta\underline{\Theta} + \delta\widetilde{\Theta}(t) \\ &= \frac{1}{f_\Theta}\left(-\delta\dot{\Theta}(t) + f_u \delta u(t)\right),\end{aligned} \tag{A. 6}$$

where $\varphi_x = \frac{f_x}{f_\Theta} > 0$ [K/ppm] is the climate sensitivity to CO_2 [34]. The bias $\delta\underline{\Theta}$ and the zero-mean component $\delta\widetilde{\Theta}(t)$, respectively, collect mean value and fluctuations of the exogenous perturbation $\delta u(t)$ and of the temperature rate $\delta\dot{\Theta}(t)$. A similar equation to (A.6) can be found in [34] and in the subsequent literature. Let us refer (A.6) as the *carbon feedback identity,* since by replacing $\delta\Theta(t)$ in (A.2), any natural exchange $v_{sh}\left(x_s, \Theta\right)$ becomes dependent on the anomaly $\delta x(t)$ of the airborne CO_2 concentration.

A.3. Differential Equations and Equilibrium

The simplest equation is that of fossil fuels. We assume that the rate $\dot{x}_5$ is only explained by anthropogenic emissions, which fact suggests the following first-order differential equation:

$$\text{Assumption 3}: \dot{x}_5(t) = -u_5(t)[\mathrm{ppm/y}],\ x_5\left(t_0\right) = x_{50}, \tag{A. 7}$$

where $u_5(t) \geq 0$ and x_{50} denote the fossil fuel reserve at time t_0. Exchange with the reservoirs $s = 2, 3, 4$ is neglected.

The first-order differential equation of a generic reservoir $s = 2, 3, 4$ explains the rate $\dot{x}_s(t)$ as the combination of the exchange with other reservoirs and of the anthropogenic emission $-u_s(t)$ to the atmosphere. We write the following:

$$\dot{x}_s(t) = \sum\nolimits_{h \neq s}\left(-v_{sh}\left(x_s, \Theta\right) + v_{hs}\left(x_h, \Theta\right)\right) - u_s(t). \tag{A. 8}$$

The atmospheric equation is similar to (A.8), but includes all the anthropogenic emissions as follows:

$$\dot{x}_1(t) = \sum\nolimits_{s=2}^{4}\left(-v_{1s}\left(x_1, \Theta\right) + v_{s1}\left(x_s, \Theta\right)\right) + \sum\nolimits_{s=2}^{5} u_s(t). \tag{A. 9}$$

We can prove that $\dot{x}_0(t) = \sum_{s=1}^{5} \dot{x}_s(t) = 0$, in agreement with the conservation equation (A.1). Equation (A.8) can be simplified by neglecting the reciprocal exchanges between $s = 2, 3, 4$, namely:

$$\text{Assumption 4}: v_{sh}(t) = 0, s, h = 2, 3, 4, s \neq h. \tag{A. 10}$$

The simplified set of equations, with $k = 2, 3, 4$, becomes the following:

$$\begin{array}{c}\dot{x}_1(t) = \sum_{s=2}^{4}\left(-v_{1s}\left(x_1, \Theta\right) + v_{s1}\left(x_s, \Theta\right)\right) + \sum_{s=2}^{5} u_s(t), x_1\left(t_0\right) = x_{10} \\ \dot{x}_k(t) = -v_{k1}\left(x_k, \Theta\right) + v_{1k}\left(x_1, \Theta\right) - u_k,\ x_k\left(t_0\right) = x_{k0} \\ \dot{x}_5(t) = -u_5(t),\ x_5\left(t_0\right) = x_{50}\end{array}. \tag{A. 11}$$

The equilibrium is obtained by setting, in (A.11), $u_s(t) = 0$ and $\dot{x}_s(t) = 0$. A pair of equilibriums can be arbitrarily chosen, for instance, the fossil fuel $\underline{x}_5$ and the overall amount $\underline{x}_0 = \sum_{h=1}^{5} \underline{x}_s$. This looks reasonable since they cannot be fixed by reciprocal exchanges, being decided by past evolution. By replacing the overall amount $\underline{x}_0$ with the atmospheric equilibrium $\underline{x}_1$, ocean, land, and cement levels can be found by the exchange equilibrium identity:

$$v_{s1}\left(\underline{x}_s, \underline{\Theta}\right) = v_{1s}\left(\underline{x}_1, \underline{\Theta}\right),\ s = 2, 3, 4. \tag{A. 12}$$

A.4 Perturbation Equation Around Equilibrium

Let us denote the column vector of the reservoir states with $\boldsymbol{x} = \left[x_1, x_2, x_3, x_4, x_5\right]$, where the inline notation [29] has been used. The equilibrium vector is denoted with $\boldsymbol{x}$ and the perturbation/anomaly with $\delta\boldsymbol{x} = \boldsymbol{x} - \boldsymbol{x}$. Clearly, $\delta\dot{\boldsymbol{x}} = \dot{\boldsymbol{x}}$. The anthropogenic exchanges $u_s, s = 2, 3, 4, 5$, are collected into the vector $\boldsymbol{u} = \left[u_2, u_3, u_4, u_5\right]$. Replacement of the expansion (A.2) into (A.11), cancellation of the constant part in (A.2) (it vanishes because of the equilibrium) and collection of the temperature perturbations terms, provides a system of state equations, which, written in the matrix form, holds:

$$\delta\dot{\boldsymbol{x}}(t) = A\delta\boldsymbol{x}(t) + G\delta\Theta(t) + \boldsymbol{B}\boldsymbol{u}(t),\ \delta\boldsymbol{x}\left(t_0\right) = \delta\boldsymbol{x}_0 \tag{A. 13}$$

The equation matrices are given by the following:

$$A = \begin{bmatrix} -k_{12}-k_{13}-k_{14} & k_{21} & k_{31} & k_{41} & 0 \\ k_{12} & -k_{21} & 0 & 0 & 0 \\ k_{13} & 0 & -k_{31} & 0 & 0 \\ k_{14} & 0 & 0 & -k_{41} & 0 \\ 0 & 0 & 0 & 0 & 0 \end{bmatrix}. \quad \text{(A. 14)}$$

$$G = \begin{bmatrix} g_1 \\ g_2 \\ g_3 \\ g_4 \\ 0 \end{bmatrix}, B = \begin{bmatrix} 1 & 1 & 1 & 1 \\ -1 & 0 & 0 & 0 \\ 0 & -1 & 0 & 0 \\ 0 & 0 & -1 & 0 \\ 0 & 0 & 0 & -1 \end{bmatrix}$$

The parameters $k_{1s}, s = 2, 3, 4$ in the first row of A correspond to the direct kinetic constant k_{dir} in (6), k_{12} refers to the reaction between atmospheric CO_2 and ocean carbonic acid as in (5), k_{13} mainly refers to photosynthesis reactions between atmospheric CO_2 and vegetation, and finally k_{14} refers to cement carbonation. They in turn become the reverse kinetic constants of the inverse reactions in the rows $s > 1$. The parameters $k_{s1}, s = 2, 3, 4$ in the first row correspond to k_{inv} in (6), namely, to the reverse kinetic constants of the reactions from atmospheric CO_2 to ocean, vegetation, soil, and cement where carbon is confined. They in turn become the direct kinetic constants of the relevant inverse reactions in the rows defined by $s > 1$. Finally, we have the identities $g_1 = \sum_{s=2}^{4} g_s$ and $g_s = -g_{1s} + g_{s1}$.

Equation (10) follows from (A.13):

1. By assuming that, during the integration interval $t_0 \le t < t_{End}$, the carbon level of ocean, land, and cement remains constant and equal to equilibrium, namely that

$$\text{Assumption 5 } : x_s(t) = \underline{x}_s,\ s = 2, 3, 4 \Rightarrow \delta x_s(t) = x_s(t) - \underline{x}_s = 0. \quad \text{(A. 15)}$$

2. By replacing $\delta\Theta$ with the carbon feedback identity (A.6) and by including $\delta\widetilde{\Theta}$ into the input w_u with the following carbon feedback assumption [34]:

$$\text{Assumption 6 } : k_{CF} = g_1 \varphi_x > 0. \quad \text{(A. 16)}$$

As a result, Eq. (A.13) reduces to a pair of equations, that of the atmospheric reservoir in (10) and that of the fossil fuel in (24). As the last assumption, null anthropogenic emissions from ocean and cement are assumed. To this end, nonzero emissions from the cement reservoir are included in u_5. The land-use change emission is decomposed into mean and zero-mean fluctuation, which implies the following:

$$\text{Assumption 7 } : u_2(t) = u_4(t) = 0, u_3(t) = \overline{u}_3 + \widetilde{u}_3(t). \quad \text{(A. 17)}$$

From (A.15) and Assumption 7, we write $u = u_5$, $w_u = \widetilde{u}_3 + g_1\delta\widetilde{\Theta}$, and we make explicit the equilibrium $\underline{x} = \left(k_{21}\underline{x}_2 + k_{31}\underline{x}_3 + k_{41}\underline{x}_4 + \overline{u}_3 + g_1\delta\underline{\Theta}\right)/k$. By denoting the net feedback gain k in (8) as $k = k_{12} + k_{13} + k_{14} - k_{CF} > 0$, by dropping the subscript $s = 1$ and by recalling the notations $r = x_5, c = u_5$ of Sect. 3.1, we obtain the following:

$$\begin{aligned} \dot{x}(t) &= -k\left(x(t) - \underline{x}\right) + u(t) + w_u(t), x\left(t_0\right) = x_0 \\ \dot{r}(t) &= -c(t), r\left(t_P\right) = r_P, t_0 < t_P < t_{End} \end{aligned}. \quad \text{(A. 18)}$$

The fossil-fuel initial time t_P corresponds to the present epoch, which implies that the initial state r_P represents the present fossil-fuel reserves, x_0 is the atmospheric CO_2 concentration at $t = t_0$, and the linear feedback term $-k\left(x(t) - \underline{x}\right)$ under $x(t) > \underline{x}$ is the effective land/ocean absorption flow corrected by the carbon feedback. Deviation from Assumption 5 in (A.15) affects the first equation in (A.18) with a model error, which is the sum of a bias $\Delta\underline{v}_{234} = k\Delta\underline{x}_{234}$ and of a zero-mean term $w_{234}(t)$. The bias is absorbed by the equilibrium $\underline{x}$, whereas $w_{234}(t)$ is absorbed by $w_u(t)$. Moreover, since $\frac{1+\tau\, k_{CF}}{\tau} = \frac{1}{\tau_{12}} + \frac{1}{\tau_{13}} + \frac{1}{\tau_{14}}$, it follows that $\tau_{1s} > \frac{\tau}{1+\tau\, k_{CF}}$, $\tau = \frac{1}{k}$, $s = 2, 3, 4$ and that $\tau\, k_{CF} \cong g$ approximates the carbon feedback gain in [34], as shown in Section 2.7.

A.5 Implications of Assumption 5

The significance of Assumption 5 in the derivation of (A.18) suggests to better grasping the relevant implications and specifically the time interval $\Delta t_m = t_m - t_0$ of the model validity. As a first step, Assumption 5 in (A.15) is rewritten by summing land, ocean, and cement carbonation CO_2 into $x_s = x_2 + x_3 + x_4$ and by relaxing the ideally zero error $\delta x_s(t)$ in (A.15) to be *nonzero but small enough* as follows:

$$\frac{\left|\delta x_s(t)\right|}{\underline{x}_s} \le \frac{1}{N_s} \ll 1, \delta x_s = x_s - \underline{x}_s, s = 234, \quad \text{(A. 19)}$$

where the upper bound $\frac{1}{N_s} \ll 1$ expresses a realistic *small enough*. As a second step, we prove that $\frac{\left|\delta x_s(t)\right|}{\underline{x}_s}$ can be upper bounded by $k_{1s}\Delta t_m \frac{\underline{x}_1}{\underline{x}_s}$, where $k_{1s} = k_{12} + k_{13} + k_{14} = k\left(1 + \frac{k_{CF}}{k}\right)$ and $\frac{\underline{x}_1}{\underline{x}_s} < 0.02$. The last inequality follows by the estimates $\frac{\underline{x}_1}{\underline{x}_2} \cong 0.02$ and $\frac{\underline{x}_3 + \underline{x}_4}{\underline{x}_2} < 0.2$ in [59]. Therefore, inequality (A.19) can be replaced by the following:

$$\Delta t_m \le \frac{\underline{x}_s}{\underline{x}_1}\frac{1}{k_{1s}N_s} \cong \frac{2.5}{k_{1s}},\ \frac{1}{N_s} = 0.05(5\%), \quad \text{(A. 20)}$$

where the upper bound value $\frac{1}{N_s} = 0.05$ (5%) has been chosen to be half than the peak 3σ uncertainty (about 10%, Table 5, row 1) of the projected CO_2 concentration.

To prove the upper bound, let us integrate the rate $\delta\dot{x}_s(t)$, which from the state equations in (A.13) and (A.18), just amounts to the land/ocean absorption rate, that is to $k_{1s}\delta x_1(t)$ plus some perturbation w_s due to linearization:

$$\delta\dot{x}_s(t) = k_{1s}\delta x_1(t) + w_s(t), \delta x_s\left(t_0\right) = \delta x_{s0}. \quad \text{(A. 21)}$$

The temperature contribution in (A.13) has been absorbed by k_{1s} (carbon feedback) and w_s. The integration in the time interval holds the following:

$$\delta x_s(\Delta t) = \Delta t_m\left(k_{1s}\overline{\delta x}_1 + \overline{w}_s\right), \quad \text{(A. 22)}$$

where overlines denote mean values in the interval $\Delta t_m = t_m - t_0$, and we assume that $\frac{|\overline{w}_s|}{k_{1s}} \ll \overline{\delta x}_1, \overline{\delta x}_1 > 0$. Since we can assume, also in the worst case of the projection 6 in Fig. 8 (the upper bound of the shaded area), the inequality $\overline{\delta x}_1 + \frac{|\overline{w}_s|}{k_{1s}} < \underline{x}_1$, we write the following:

$$\frac{|\delta x_s(t)|}{\underline{x}_s} < k_{1s}\Delta t_m \frac{\underline{x}_1}{\underline{x}_s}, \quad \text{(A. 23)}$$

and we replace (A.19) with $k_{1s}\Delta t_m \frac{\underline{x}_1}{\underline{x}_s} \leq \frac{1}{N_s} \ll 1$. In turn, the latter inequality can be converted into (A.20). By posing $k_{1s} \cong \widehat{k} = 0.019$ ($\pm 0.0016, 1\sigma$) y^{-1} (Table 3, Section 2.5), we find out $\Delta t_{m,-3\sigma} = 105 \leq \Delta t_m \leq \Delta t_{m,+3\sigma} = 176$ y (3σ), just below the projection interval $t_{End} - t_0 = 2150 - 1955 = 195$ y.

Author Contribution E.C.: development, identification, and analysis of mathematical models, simulation and analysis of results. D.M.: development of chemical equations and mathematical models. C.N.: analysis of mathematical models and of simulation results, coordination of the project.

Funding Open access funding provided by Politecnico di Torino within the CRUI-CARE Agreement.

Data Availability A package with MATLAB Live Script, input/output data, check results and guidelines is available at the repository https://github.com/carlovnovara/PolitoCliDyn/tree/1storderCC.

Declarations

Ethics Approval This study does not require any Ethical Approval.

Conflict of Interest The authors declare no conflict interests.

References

1. IPCC. (2022). Summary for Policymakers. In P.R. Shukla et al. (Eds.), *Climate Change 2022: mitigation of climate change. Contribution of Working Group III to the Sixth Assessment Report of the Intergovernmental Panel on Climate Change*, Cambridge, UK, Cambridge University Press, https://doi.org/10.1017/9781009157926.001.
2. Houghton, J. T., Jenkins, G. J., & Ephraums, J. J. (1990). *Climate change*. Cambridge, UK, Cambridge University Press.
3. Climate Action Tracker. (2024). *Global temperatures, addressing global warming,* dataset retrieved April 10, 2024 from https://climateactiontracker.org/global/temperatures/.
4. Arias P.A. et al. (2021). Technical Summary. In *Climate Change 2021: The Physical Science Basis. Contribution of Working Group I to the Sixth Assessment Report of the Intergovernmental Panel on Climate Change,* V. Masson-Delmotte et al. (Eds.), Cambridge, UK, Cambridge University Press, 33–144. https://doi.org/10.1017/9781009157896.002.
5. Sterman, J., et al. (2014). WORLD CLIMATE: a role-play simulation of climate negotiations. *Simulation and Gaming,46*(4), 1–35.
6. Sterman, J., Fiddaman, T., Franck, T., & Jones, A. (2012). Climate interactive: the C-ROADS climate policy model. *System Dynamics Review*. https://doi.org/10.1002/sdr.1474
7. Eyring, V., et al. (2016). Overview of the couple model intercomparison project phase 6 (CMIP6) experimental design and organization. *Geoscientific Model Development,9*(5), 1937–1958. https://doi.org/10.5194/gmd-9-1937-2016
8. Meinshausen, M., et al. (2011). The RCP greenhouse gas concentrations and their extensions from 1765 to 2300. *Climate Change,109*, 213–241. https://doi.org/10.1007/s10584-011-0156-z
9. IPCC. (2021). Annex II: Models [J.M. Gutierrez et al. (eds.)]. In *Climate Change 2021: The Physical Science Basis. Contribution of Working Group I to the Sixth Assessment Report of the Intergovernmental Panel on Climate Change,* V. Masson-Delmotte et al. (Eds.), Cambridge, UK, Cambridge University Press, 2087–2138.https://doi.org/10.1017/9781009157896.016.
10. Ward, J. D., Warner, A. D., Nel, W. P., & Beecham, S. (2011). The influence of constrained fossil fuel emissions scenarios in climate and water resource projection. *Hydrology and Earth System Science,15*, 1879–1893. https://doi.org/10.5194/hess-15-1879-2011
11. Tans, P. (2009). An accounting of the observed increase in oceanic and atmospheric CO2 and an outlook for the future. *Oceanography,22*(6), 26–35. https://doi.org/10.5670/oceanog.2009.94
12. Karecha, P.K., & Hansen, J.E. (2012). Implications of "peak oil" for atmospheric CO_2 and climate. *Global Biogeochemical Cycles,* 22. https://doi.org/10.1029/2007GB003142.
13. Vernon, C., Thompson, E., & Cornell, S. (2011). Carbon dioxide emission scenario: limitations of the fossil fuel resource. *Procedia Environmental Sciences,64*, 206–215. https://doi.org/10.1016/j.proenv.2011.05.022
14. Brecha, R.J. (2008). Emissions scenarios in the face of fossil fuel peaking, *Physics Faculty Publications*, 23, document retrieved September 1, 2023 from https://ecommons.udayton.edu/phy_fac_pub/23.a.
15. Moss, R. H., et al. (2010). The next generation scenarios for climate change research and assessment. *Nature,463*, 747–756. https://doi.org/10.1038/nature08823

16. McGlade, C., & Ekins, P. (2015). The geographical distribution of fossil fuels unused when limiting global warming to 2°C. *Nature,517*, 187–190. https://doi.org/10.1038/nature14016
17. Welsby, D., Price, J., Pye, S., & Ekins, P. (2021). Unextractable fossil fuels in a 1.5°C world. *Nature,597*, 230–234. https://doi.org/10.1038/s41586-021-03821-8
18. Keeling, C. D. (1960). The concentration and isotopic abundances of carbon dioxide in the atmosphere. *Tellus,12*(2), 200–203. https://doi.org/10.1111/j.2153-3490.1960.tb01300.x
19. Tans, P., & Thoning, K. (2018). How we measure background CO2 levels on Mauna Loa, *NOAA Earth System Research Laboratory.* document retrieved September 19, 2023 from https://gml.noaa.gov/ccgg/about/co2_measurements.html
20. IPCC (2021). Annex VII: Glossary [Matthews, J.B.R. et al. (eds.)]. In *Climate Change 2021: The Physical Science Basis. Contribution of Working Group I to the Sixth Assessment Report of the Intergovernmental Panel on Climate Change,* V. Masson-Delmotte et al. (Eds.), Cambridge, UK, Cambridge University Press, 2215–2256. https://doi.org/10.1017/9781009157896.022.
21. Archer, D. (2010). *The Global Carbon Cycle*. Princeton.
22. Canadell, J.C. et al. (2021). Chapter V: Global carbon and other biogeochemical cycles and feedbacks. In *Climate Change 2021: The Physical Science Basis. Contribution of Working Group I to the Sixth Assessment Report of the Intergovernmental Panel on Climate Change,* V. Masson-Delmotte et al. (Eds.), Cambridge, UK, Cambridge University Press, 673–816.https://doi.org/10.1017/9781009157896.007.
23. Mazza, D., & Marino, F. (2021). *La strega perfetta, fatti e misfatti della CO2 (in Italian)*. Italy, TabEdizioni.
24. Global Carbon Project (2023). *Global Carbon Budget Data*, dataset retrieved September 19, 2023 from https://www.globalcarbonproject.org/carbonbudget/22/data.htm.
25. Friedlingstein, P., et al. (2022). Global Carbon Budget 2021. *Earth Syst. Sci. Data,14*, 1917. https://doi.org/10.5194/essd-14-1917-2022
26. Scripps Research CO_2 Program. (2023). *Atmospheric CO_2 Data, Ice-core Merged Products,* dataset retrieved September 19, 2023 from https://scrippsco2.ucsd.edu/data/atmospheric_co2/icecore_merged_products.
27. Callendar, G. S. (1938). The artificial production of carbon dioxide and its influence on temperature. *Quarterly Journal of Royal Meteorological. Society,64*, 223–237. https://doi.org/10.1002/qj.49706427503
28. Dittberner, G. J. (1978). Climatic change: volcanoes, manmade pollution and carbon dioxide. *IEEE Trans. Geoscience Electronics,16*(1), 50–61. https://doi.org/10.1109/TGE.1978.294525
29. Canuto, E., Novara, C., Massotti, L., Carlucci, D., & Perez, M. C. (2018). *Spacecraft Dynamics and Control: The Embedded Model Control Approach*. UK, Butterworth-Heinemann.
30. Mazza, D., & Canuto, E. (2022). *Fundamental Chemistry with Matlab, Amsterdam, the Netherlands*. Elsevier.
31. Broecker, W. S., & Peng, T.-H. (1982). *Tracers in the Sea*. NY, Lamont-Doherty Geological Observatory, Columbia University.
32. Plumb, R.A., & Stolanski, R.S. (2013). The theory of estimating lifetimes using model and observations, Chapter 2. *SPARC Lifetimes Report*, Report No. 6.
33. Meinshausen, M., Raper, S. C. B., & Wigley, T. M. L. (2011). Emulating coupled atmosphere-ocean and carbon cycle models with a simpler model, MAGICC6 – Part 1: Model description and calibration. *Atmospheric Chemistry and Physics,11*(4), 1417–1456. https://doi.org/10.5194/acp-11-1417-2011
34. Friedlingstein, P., Dufresne, J. L., Cox, P. M., & Rayner, P. (2003). How positive is the feedback between climate change and the carbon cycle? *Tellus B: Chemical and Physical Meteorology,55*(2), 602–700. https://doi.org/10.3402/tellusb.v55i2.16765
35. PAGES 2K Consortium. (2019). Consistent multi-decadal variability in global temperature reconstructions and simulations over the Common Era. *Nature Geoscience,12*(8), 643–649. https://doi.org/10.1038/s41561-019-0400-0
36. Williams, R. G., Katavouta, A., & Goodwin, P. (2019). Carbon-cycle feedbacks operating in the climate system. *Current Climate Change Reports,5*, 282–295. https://doi.org/10.1007/s40641-019-00144-g
37. Zhang, X., et al. (2021). A small climate-amplifying effect of the climate-carbon cycle feedback. *Nature Communications,12*(2952), 1–11. https://doi.org/10.1038/s41467-021-22392-w
38. Novara, C., Mazza, D., & Canuto, E. (2023). Land/ocean absorption dynamics and airborne projection of carbon dioxide under finite fossil-fuel reserves. *IFAC-PapersOnLine, 56*(2), 8302–8307. https://doi.org/10.1016/j.ifacol.2023.10.1018
39. Fisher, M. J. (2014). *Generalized hyperbolic secant distributions: With applications to finance*. Springer.
40. Trenberth, K. E., & Smith, L. (2005). The mass of the atmosphere: A constraint on global analyses. *Journal of Climate,18*, 864–875. https://doi.org/10.1175/JCLI-3299.1
41. Zeebe, R.E., & Wolf-Glabrow, D. (2001). *CO_2 in seawater: equilibrium, kinetics, isotopes*. Amsterdam, the Netherlands, Elsevier.
42. Emerson, S. R., & Hedges, J. I. (2008). *Chemical oceanography and the marine carbon cycle*. UK, Cambridge University Press.
43. Friedlingstein, P. (2015). Carbon cycle feedbacks and future climate change. *Philosophical Transactions of the Royal Society A,335*(20140421), 1–14. https://doi.org/10.1098/rsta.2014.0421
44. Revelle, R., & Suess, H. E. (1957). Carbon dioxide exchange between atmosphere and ocean and the question of an increase of atmospheric CO2 during the past decades. *Tellus,9*(81), 18–27. https://doi.org/10.1111/j.2153-3490.1957.tb01849.x
45. Connolly, R., Connolly. M., Carter, R.M., and Soon, W. (2020). How much human-caused global warming should we expect with business-as-usual (BAU) climate policies? A semi-empirical assessment, Energies, 13 (6), paper 1365, https://doi.org/10.3390/en13061365.
46. NOAA Global Monitoring Laboratory (2023). Trends in atmospheric carbon dioxide. retrieved September 19, 2023 from https://gml.noaa.gov/ccgg/trends/data.html
47. Jones, C. D., & Cox, P. M. (2001). Modeling the volcanic signal in the atmospheric CO2 record. *Global Biogeochemical Cycles,15*(2), 453–465. https://doi.org/10.1029/2000GB001281
48. Neftel, A., Moor, E., Oeschger, H., & Stauffer, B. (1985). Evidence from polar ice cores for the increase in atmospheric CO2 in the past two centuries. *Nature,315*, 45–47. https://doi.org/10.1038/315045a0
49. IPCC (2001). *Climate Change 2001: The Scientific Basis. Contribution of Working Group I to the Third Assessment Report of the Intergovernmental Panel on Climate Change,* J.T. Houghton et al. (Eds.), Cambridge University Press, Cambridge, UK.
50. Millar, J. R., Nicholls, Z. R., Friedlingstein, P., & Allen, M. R. (2017). A modified impulse-response representation of the global near-surface air temperature and atmospheric concentration response to carbon dioxide emissions. *Atmospheric Chemistry and Physics,17*, 7213–7228. https://doi.org/10.5194/acp-17-7213-2017
51. Bebbington, J., Schneider, T., Stevenson, L., & Fox, A. (2020). Fossil-fuel reserves and resources reporting and unburnable carbon: investigating conflicting accounts. *Critical Perspectives on Accounting,66*, 1–22.
52. Our World in Data (OWID) (2023). *Fossil fuels data explorer,* dataset retrieved July 30, 2023 from https://ourworldindata.org/explorers/natural-resources
53. Climate Interactive (2023). *The EN-ROADS climate solutions simulator*, document retrieved September 1, 2023 from https://www.climateinteractive.org/en-roads/.
54. CO2-Earth (2023). *CO2 Future*, *2100 Projections,* dataset retrieved August 20, 2023 from https://www.co2.earth/2100-projections.
55. IPCC (2011). Annex III: Tables of historical and projected well-mixed greenhouse gas mixing ratios and effective radiative forcing of all climate forcers [F.J. Dentener et al. (eds.)]. In *Climate Change 2021: The Physical Science Basis. Contribution of*

Working Group I to the Sixth Assessment Report of the Intergovernmental Panel on Climate Change, V. Masson-Delmotte et al. (Eds.), Cambridge, UK, Cambridge University Press. 2139–2152. https://doi.org/10.1017/9781009157896.017

56. International Institute for Applied Systems Analysis (IIASA) (2023). SSP Database (Shared Socioeconomic Pathways)-Version 2.0, dataset retrieved September 22, 2023 from https://tntcat.iiasa.ac.at/SspDb/dsd?Action=htmlpage&page=10
57. The University of Melbourne. (2023). Greenhouse gas concentrations, carbon dioxide. dataset retrieved September 22, 2023 from https://greenhousegases.science.unimelb.edu.au/#!/ghg?mode=downloads
58. Canuto E., Mazza, D., & Novara, C. (2024). A second-order dynamic model of the mean global carbon cycle, to appear in IFAC-PapersOnLine, proceedings of the 3 IFAC Workshop on Integrated Assessment Modeling for Environmental Systems, IAMES 2024, Savona, Italy, 29–31 May 2024.
59. World Ocean Review. (2023). Ocean chemistry. retrieved September 22, 2023 from https://worldoceanreview.com/en/wor-1/ocean-chemistry/co2-reservoir/